

Recommended initial precession phase for Gaia Scanning Law

prepared by: S.A. Klioner, F. Mignard
affiliation : LO
reference: GAIA-C3-TN-TUD-SK-018-1
issue: 1
revision: 1
date: 2014-02-03
status: Issued

Abstract

Report on the recommended value for the initial precession phase for the Gaia Scanning Law. The report summarizes the general principles applied to optimize the scanning law for the planned relativistic tests of the quadrupole light deflection due to Jupiter and provides details of the procedure we applied to validate the software and select the optimal initial precession phase. The recommended value for the initial precession phase is $\nu_0 = 52.66°$.

Document History

Issue	Revision	Date	Author	Comment
1	1	2014-01-28	SK&FM	Issued to the Livelink
D	0	2014-01-28	SK&FM	Distributed for comments
D	0	2014-01-02	FM	Start of the document

Contents

1 Notations **10**

2 Introduction **10**

3 Principles of the optimization **11**
3.1 Noise models 11

4 Qualifications of the software **12**
4.1 Validation of the software 12
4.2 Validation of the Gaia orbit 16
4.3 Validation of the scanning law 19

5 Conventions for the initial conditions of the scanning law **19**

6 Selection of good initial precession **20**
6.1 The period of the search for the GAREQ-relevant observations 20
6.2 The selection criteria 21
6.3 Selection of the potentially good areas 25
6.4 Ranking of the candidate solutions 39
6.5 Check with ALADIN on few prominent stars 40
6.6 Recommendation of a precession initial value 41

7 Relevant observations for the recommended initial precession phase **45**

8 Evaluation of possible spin phase maneuvers for the selected point **49**

9 Sensitivity to assumptions **52**
9.1 Noise model 52
9.2 Gaia orbit 52
9.3 Scan rate 53

10 Computational aspects and online repository **60**

A Summary of individual observations **62**

List of Figures

1 Adopted AL location estimation performance 12
2 Comparison of the color-coded maps produced by SOGAR in Java and Fortran 15
3 Visualization of the delivered Gaia orbit 17
4 Errors in Gaia position between the MOC orbit file and the GaiaTools 18
5 Errors in Gaia position between the MOC orbit file and the Fortran code 18
6 Four angles used in the formulation of the scanning law 20
7 Distribution of the s/n ratios over a typical grid 24
8 The map of the s/n ratio for N_1 and full AC extension 26
9 The map of the s/n ratio for N_1 and the AC extension of 70% 27
10 The map of the s/n ratio for N_2 and full AC extension 28
11 The map of the s/n ratio for N_2 and the AC extension of 70% 29
12 The map of the s/n ratio for N_3 and full AC extension 30
13 The map of the s/n ratio for N_3 and the AC extension of 70% 31
14 Regions of interest on the colour-coded maps 32
15 The map of the s/n ratio in region 2 for N_1 and full AC extension 33
16 The map of the s/n ratio in region 2 for N_1 and the AC extension of 70% 34
17 The map of the s/n ratio in region 2 for N_2 and full AC extension 35
18 The map of the s/n ratio in region 2 for N_2 and the AC extension of 70% 36
19 The map of the s/n ratio in region 2 for N_3 and full AC extension 37
20 The map of the s/n ratio in region 2 for N_3 and the AC extension of 70% 38
21 ALADIN screenshot around the star with $\alpha = 201.4053°$, $\delta = -7.3830°$ 42
22 ALADIN screenshot around the star with $\alpha = 228.6469°$, $\delta = -17.2359°$ . . . 43
23 ALADIN screenshot around the star with $\alpha = 263.6591°$, $\delta = -22.6800°$ . . . 44
24 The close approach of Jupiter in February 2017 with a star of magnitude ≈ 13 . 47
25 Close-up view of the close approach in February 2017 48
26 The effect of spin-phase maneuvers for the selected initial conditions 51
27 Difference between two releases of the Gaia orbit 53
28 The s/n ratio as function of scan rate for N_1 56
29 The s/n ratio as function of scan rate for N_2 57
30 The s/n ratio as function of scan rate for N_3 58
31 Best s/n ratio as function of the scan rate 59

List of Tables

1 Notations used in this document 10
2 Summary of the colour-coded maps 25
3 Summary of the colour-coded maps for region 2 32
4 Ranking of the candidate solutions 39
5 Recommended initial conditions 41
6 The most favourable events for the selected initial conditions 46
7 The effects of spin phase maneuvers 50

8 The gain due to spin phase maneuvers 50

Acronyms

The following table has been generated from the on-line Gaia acronym list:

Acronym	Description
2MASS	Two-Micron All Sky Survey
AC	across scan
AGIS	Astrometric Global Iterative Solution
AL	along scan
CCD	Charge-Coupled Device
CDS	Centre de Données astronomiques de Strasbourg (Strasbourg astronomical Data Center)
CPU	Central Processing Unit
DLR	Deutsches Zentrum für Luft und Raumfahrt
DPAC	Data Processing and Analysis Consortium
DPACE	Data Processing and Analysis Consortium Executive
DSS	Digitized Sky Survey
EPS	Electrical Power Sub-system
EPSL	Ecliptic Pole Scanning Law
ESA	European Space Agency
ESOC	European Space Operations Centre (ESA)
FOV	Field of View (also denoted FOV)
FoVRS	Field-of-View Reference System
GAREQ	GAia Relativistic Experiment on Quadrupole light deflection
GGU	Global Generic Update
GPDB	Gaia Parameter DataBase
GREM	Gaia RElativity Model
IOCR	In-Orbit Commissioning Review
JD	Julian Date
MOC	Mission Operations Centre
MSL	Modified Scanning Law
NSL	Nominal Scanning Law
PC	Project Coordinator
PS	Project Scientist
REMAT	RElativistic Models And Tests (DU in CU3)
RRFWG	Relativity and Reference Frame Working Group (precursor of REMAT)
RSLS	Reference Scanning Law Schedule
SL	Scanning Law
s/n	signal-to-noise (ratio)
SOC	Science Operation Centre

SOGAR	Scanning-law Optimization for GAREQ
TCB	Barycentric Coordinate Time
TDB	Barycentric Dynamical Time (obsolete)
TYC	TYCHO (stellar calatog)
ZARM	Centre for Applied Space Dynamics and Microgravity, Bremen (Germany)

References

[JDB-053], de Bruijne, J., 2009, *ALong- and ACross-scan location-estimation performance*, GAIA-CA-TN-ESA-JDB-053, URL http://www.rssd.esa.int/cs/livelink/open/2913726

[ESA-SCI(2000)4], GAIA Science Advisory Group, 2000, *GAIA. Composition, Formation and Evolution of the Galaxy [The GAIA Study Report (ESA-SCI(2000)4)]*, ESA-SCI(2000)4, URL http://www.rssd.esa.int/cs/livelink/open/359232

[JMF-003], Martin Fleitas, J., Mora, A., Raison, F., et al., 2011, *VPU. Object detectability near bright extended sources. The Jupiter case*, GAIA-CH-TN-ESAC-JMF-003, URL http://www.rssd.esa.int/cs/livelink/open/3061697

[FM-037], Mignard, F., 2012, *Validation of the analytical NSL for the Jupiter experiment*, GAIA-CA-TN-OCA-FM-037, URL http://www.rssd.esa.int/cs/livelink/open/2888916

[HS-003], Siddiqui, H., 2012, *Gaia mission scheduling and optical observation ICD*, GAIA-C1-SP-ESAC-HS-003, URL http://www.rssd.esa.int/cs/livelink/open/2954990

[HV-022], Voss, H., Jordi, C., et. al. Fabricius, C., 2013, *Optimizing the gating strategy for AF*, GAIA-CH-TN-UB-HV-022, URL http://www.rssd.esa.int/cs/livelink/open/3234092

U. Abbas, M. Lattanzi, M.T. Crosta, Optimizing the scanning law parameters for GAREQ using QFIND, GAIA-C3-TN-INAF-UA-004-D, draft.

G. Anglada Escudé, Experiments and relativistic models for optical astrometry in space, PhD thesis, Universitat de Barcelona, June 2007

G. Anglada Escudé, S. Klioner and J. Torra, Relativistic light deflection near giant planets using Gaia astrometry, Proceedings of the Eleventh Marcel Grossmann Meeting on General Relativity, ed. by H. Kleinert, R.T. Jantzen and R. Ruffini, World Scientific, Singapore, Part C, 2588, 2007

M. T. Crosta and F. Mignard, *Classical and Quantum Gravity* **23**, 4853 (2006).

S. A. Klioner, Soviet Astronomy, 35, 523-530, 1991 (Astronomicheskij Zhurnal, 68(5), 1046-1062, 1991, in Russian)

S.A. Klioner, In: Lasers, Clocks and Drag-Free: Exploration of Relativistic Gravity in Space, H. Dittus, C. Lämmerzahl, S. G. Turyshev (eds.), Proc. of the International Conference, ZARM, University of Bremen, May 2005, Astrophysics and Space Science Library 349, Springer, Berlin, 399-426, 2007

S.A. Klioner, Astronomical Journal, 125(3), 1580-1597, 2003

F. Mignard, S.A. Klioner, Ch. Ordenovic, NSL Optimization for Quadrupole Experiment(SOGAR), GAIA-C3-TN-OCA-FM-050-D, in preparation

F. Mignard, Ch. Ordenovic, SOGAR Status Presentation at the REMAT-12 meeting, 11-12 July 2013. `http://gaia.esac.esa.int/dpacsvn/DPAC/meetings/CU3/REMAT/12-Paris-Jul-13/FM_REMAT12_SOGAR.pdf`

1 Notations

The main mathematical notations used in this report are summarized in Table 1.

Symbol	Meaning
ω	spin rate, arcsec/s (deg/h)
Ω	spin phase, degrees
Ω_0	initial spin phase at reference epoch, degrees
ν	precession phase, degrees
ν_0	initial precession phase at reference epoch, degrees
$T_{\rm ref}$	reference epoch for the initial phases: 1 Sep 2013, 0h TCB, JD = 2456536.5 TCB
s/n	a short-hand for the merit function or the efficiency factor

TABLE 1: Notations used in this document

2 Introduction

Relativistic tests with Gaia belong to the initial proposal and appears in the early compilation of the science objectives published in 2000 ESA-SCI(2000)4. Several ideas were already circulating that time primarily based on the light deflection by the Sun and to a lesser extent by the giant planets. The gravitational deflection of light due to the giant planets is integral part of the GREM model (Klioner, 2003). GREM includes also the model for the deflection of light due to the quadrupole gravitational fields of giant planets as developed in Klioner (1991). All the effects included in the model can be used to test their presence in the observational data. In this way a series of planned relativistic tests with Gaia data were formulated (Klioner, 2007). Realistic possibilities of Gaia to detect the quadrupole deflection of light from Jupiter was investigated in more detail by Anglada & Klioner, and Crosta & Mignard. Both groups showed the opportunity offered by Gaia outstanding astrometry to detect this minute deflection, reaching at maximum 240 μas for a grazing ray. Analysis shows that Gaia will only be able to **detect** the effect with a $\sim 3-9\,\sigma$ level. One should notice that if the effect is detected, it would not be a stringent test of general relativity, but this will be a remarkable achievement illustrating the power of astrometric measurements to contribute to fundamental physics. This would be the detection of a predicted phenomena that has never been observed, and actually could not have been until Gaia (Anglada, 2007; Anglada et al., 2007; Crosta and Mignard, 2006).

To have a chance to perform such a detection one needs to carry out astrometric measurements on bright stars when they are nearly aligned with Jupiter at some epochs and far from Jupiter at most of the other epochs. Given the way Gaia scans the sky, these opportunities could only happen when Jupiter is in one of the Gaia viewing directions. Since these are rare events, a

question arises immediately: could we plan the scanning in order to observe Jupiter with Gaia when it moves past a bright star? Since the scanning law has two free parameters, virtually unconstrained, it is tempting to use this freedom to increase the science return and select the values of these parameters that maximize the level of detection of the quadrupole light deflection. This is precisely what is behind the expression *NSL optimization*.

3 Principles of the optimization

Basically the software SOGAR designed to optimize the scanning law explores a grid of initial conditions, initial precession and spin phases, and determines for every grid point how well the detection of the Jupiter quadrupole light deflection could be ascertained from the observations of bright stars close to the limb of Jupiter. This computer package is a simulator, which determines all the occurrences of Jupiter transits in the Gaia FOVs using the adopted scanning law and the orbits of Gaia and Jupiter. For each transit the stars up to a certain magnitude are extracted from a stellar catalogue and examined one by one to see whether they are good candidates to detect the light deflection. The star must be relatively bright for the astrometry, but not too bright, close to Jupiter, i.e at less that 2 or 3 Jupiter radii from the planet disk projected on the sky and the deflection vector must have the largest possible projection on the along-scan direction.

The relative merit of each occurrence is evaluated by comparing the magnitude of the deflection projected on the AL direction to the astrometric AL accuracy of a single observation for this particular star. When all the Jupiter transits for a grid point of initial condition are exhausted the value of this particular choice is quantified by summing up the individual merit values. In the detail the software contains many shortcuts and optimization to speed up the process since the number of grid points to be looked at is very large in the operational version. Each initial conditions must be sampled from 0 to 360 degrees with a step size of 0.2 degrees, meaning in total more than 3 millions instances. For each case, the Jupiter transits must be found over 5 years, and for each transit, several tens or hundreds of stars must be investigated. The calculations must be done with a number of noise models and a number of variants with some other parameters to meet the current uncertainties with Gaia actual performance and implementation. A detailed presentation of the algorithms and of their implementations can be found in Mignard et al. (2014).

3.1 Noise models

Three noise models were considered in this investigation:

N_0 The noise model which resembles the along-scan location estimation performance as described in JDB-053 (the gating scheme was updated in HV-022). This noise model gives the AL error as function of G magnitude only. We decided to be more conservative with the gated stars and adopted the noise model shown as green line in Figure 1. The noise

model N_0 was not directly used for the SOGAR runs, but only as models N_2 and N_3 described below.

N_1 The noise model with the straylight from Jupiter JMF-003 and with a star considered as not observable if it is closer than $2''$ to the Jupiter limb (sometimes denoted as the model "straylight2"). This is the most "pessimistic" noise model predicting smallest s/n ratios for the quadrupole deflection of light. The details how the analysis of JMF-003 has been adapted to SOGAR is explained in (Mignard et al., 2014).

N_2 The "plain" noise model N_0 based only on the magnitude of the star with a star considered as not observable if it is closer than $5''$ to the Jupiter limb (sometimes denoted as the model "plain5").

N_3 The "plain" noise model N_0 based only on the magnitude of the star with a star considered as not observable if it is closer than $2''$ to the Jupiter limb (sometimes denoted as the model "plain2"). This is the most "optimistic" noise model predicting largest s/n ratios for the quadrupole deflection of light.

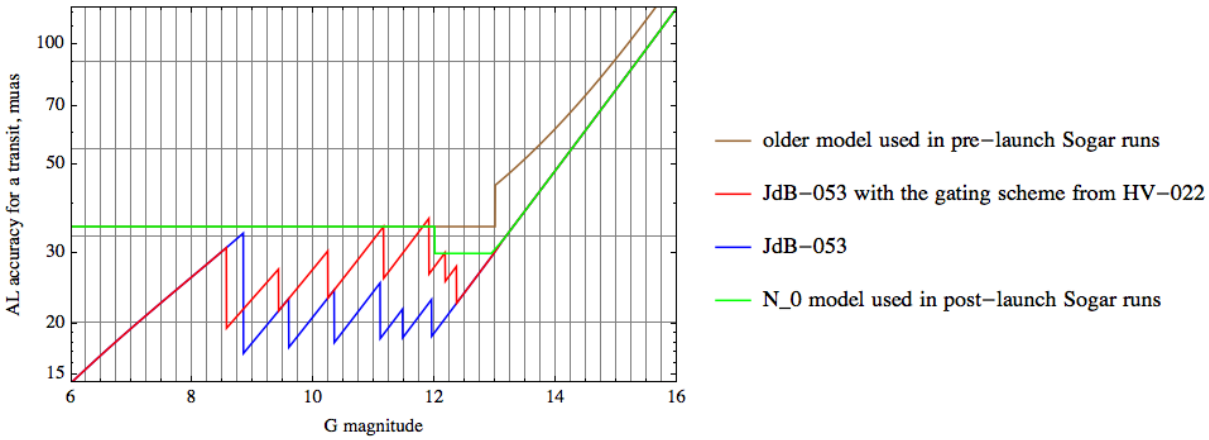


FIGURE 1: Graphical representation of the along-scan location estimation performance as function of the magnitude. The model shown in green is used for the post-launch SOGAR runs relevant for this report.

4 Qualifications of the software

4.1 Validation of the software

Two versions of the software has been produced and used to select the recommended values of the initial conditions. One is SOGAR/Fortran which was historically the development version from which the algorithms were evaluated and tested as of 2008. The second is the official Java version, integrated in the REMAT environment and ultimately the only one used to produce the reference data. Although these are two different implementations, the underlying algorithms

are very similar, since the first version of the SOGAR/Java was just a translation from Fortran to Java. However the two architectures are not identical:

- In the Fortran version, the list of transits of Jupiter are first computed over the whole period (nominally 5 years, but the actual duration is a configuration parameter) and stored as an intermediate file. This depends on the orbits of Gaia and Jupiter and on the scanning law. All the transits are computed for each grid point of initial conditions. For each grid point one has on the average 65 Jupiter transits. For a grid exploration with steps of 1° in precession and spin phases, we then have typically $360^2 \times 65 \simeq 8.5$ millions records in this file. Then a second program is run to investigate the star field around Jupiter and compute the merit function of each transits according to the noise model. This approach is very useful to study the impact of the noise, the selection of the star catalogue, the brightness limit on the result, without recomputing the transits, since producing the list of transits is much longer than the appraisal of the value of a grid point. This break between two different programs allows an interesting check, since the crossing times of Jupiter are read from the output of the first program and used to determine the star field in the Gaia FOV at this time. Therefore the location of Jupiter is computed again in a direct way instead of within the process of searching the transit time. At this time Jupiter must be in the FOV with an AL $\eta \simeq 0$. A warning is issued if this is not the case.
- The Java version is more integrated and at each launch one computes in a single big loop the transits for a particular initial condition and evaluates its merit. With this version it is easier to change the grid sampling, since it does not use a precomputed transit file, but any test with a new noise model needs to restart the whole run.

Another important difference between the two versions is that the Fortran version does not use the MSL which is a pure Java product available in the Gaia Tools. The analytical approximation NSL037 is used instead, (FM-037) and it is known that the analytical and numerical version are consistent within less than $10''$ in pointing directions[1]. Since the SOGAR/Java can also run on the NSL037, detailed comparisons could be made between the Java and Fortran version. This is done on a regular basis, as often as possible, and in particular with the operation orbit used to produce the final selection of the recommended initial conditions. In short, the two versions produce exactly the same results for identical settings. This feature, which was costly in terms of human effort, proved an essential asset to detect anomalies, which would have gone unnoticed otherwise. Both versions benefited from its companion. Detailed reports on how the perfect identity was achieved, and why it was not straightforward, can be found in the SOGAR presentations done at every REMAT meeting since 2008 and in Mignard et al. (2014).

During this final selection in the first week of January 2014, we (SK and FM) ran the two versions with SL037 for the scanning law and the predicted orbit of Gaia provided by MOC

[1] Since then a numerical version of the scanning law has been implemented as well in the Fortran version which is in full agreement with the Java version to the sub-mas level. However it has not been used in the work reported in this note.

(see Section 4.2) until we arrived at the same results: same values of the merit functions over the grid of initial conditions, the same stars seen around Jupiter at the same distance and with identical geometry, etc. All differences found during this exercise were traced back quickly to different parameter settings and fixed.

The identity of the two exploitations (Java and Fortran) with the analytical scanning law and the same setting for the other configurations parameters is illustrated in Figure 2. The colour plot displays the map of the level of detection (the s/n ratio) of Jupiter quadrupole light deflection as a function of the initial conditions of the scanning law. The analytical scanning law NSL037 has been used in both cases, with the Java and Fortran implementation of SOGAR and the same noise models. Since the plots are not produced by the same software, the colour scale has been adapted to better evidence the similarity of the overall maps and one can see in the headers that the maximum and minimum values are identical.

During the development phase comparisons with another independent software written to prepare one aspect of the scientific exploitation of the Jupiter light deflection data and written by U. Abbas (Abbas et all., 2014) helped to strengthen our confidence in one of the critical steps of the program which determines the times when one of the Gaia FOVs is pointing to Jupiter. Although limited to the nominal parameters of the scanning law, reaching the identity in crossing times and location in the FOV brought another proof of the correctness of the implementation.

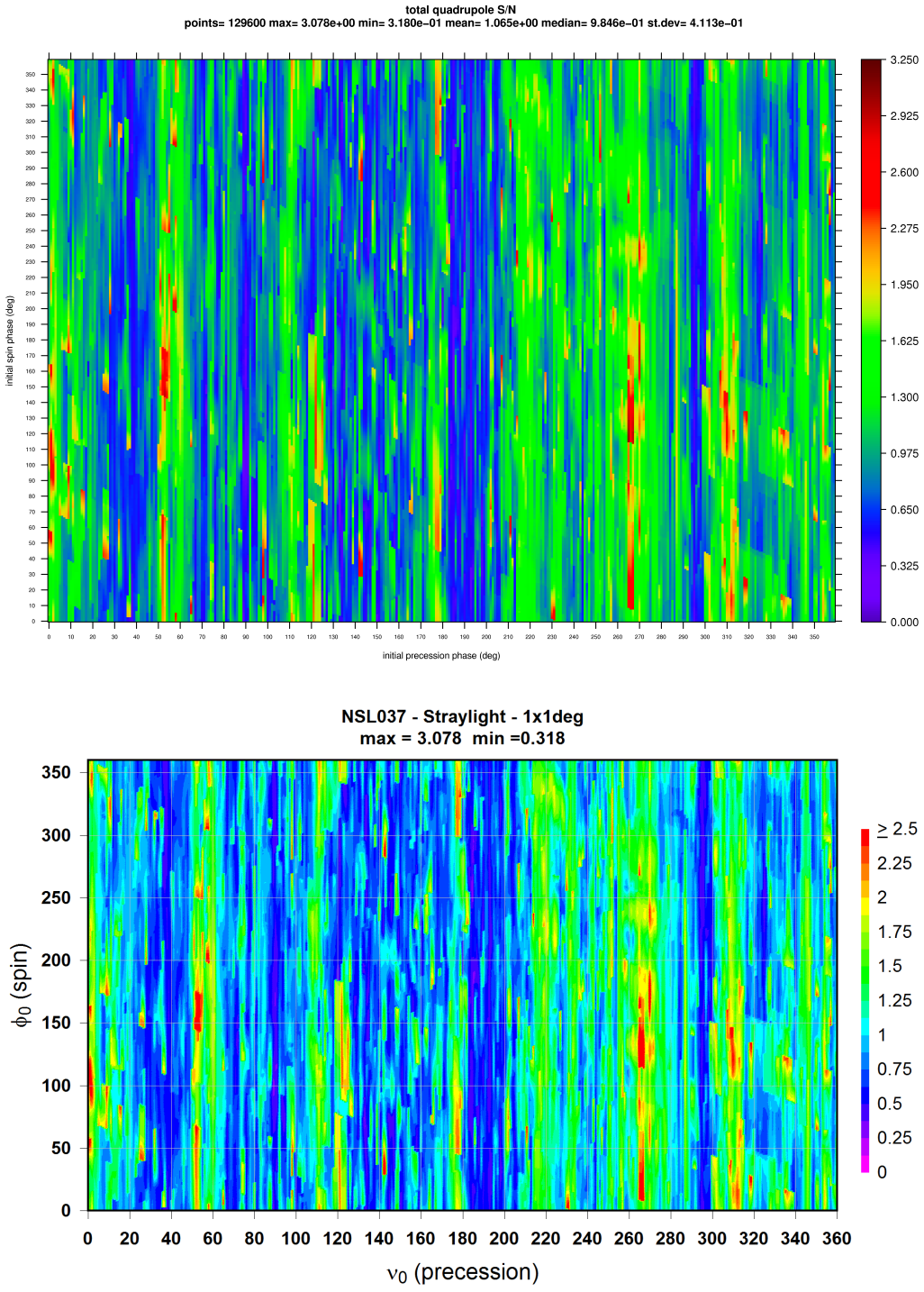


FIGURE 2: Comparison of the final map of the s/n ratio for the detection of the light deflection by the quadrupole moment of Jupiter. The upper map is produced with the Java version of SOGAR and the lower one with the Fortran version.

4.2 Validation of the Gaia orbit

The predicted orbit was received from MOC at SOC on 30 December 2013 and processed with the orbit importer to generate a gbin file readable by the Java program. It was made available to us on 31 December 2013 by SOC. The gbin file was carefully validated. First, the orbit as given in gbin was visualized to see that the orbit is really a Lissajous one around L_2 (see Figure 3). The orbit in the gbin file and the GaiaTools implementation of the orbit was then directly checked against the orbit file delivered by the MOC with a step size of 1 sec (Figure 4). The comparison shows that the formal numerical errors of the gbin file, as expected, do not exceed 1 metre.

For the Fortran version this orbit is re-fitted into a set of Chebyshev coefficients compatible with the ephemeris library used by SOGAR/Fortran. Given the sensitivity of SOGAR results to the Gaia orbit, we deemed necessary to check whether also the Fortran implementation of the orbit used in the SOGAR software is in agreement with the orbit data delivered by MOC. This was done by comparing at sample times our computed positions (and velocities) of Gaia from the Earth barycentre to a set of reference positions (and velocities) provided by MOC and covering the $\sim$ 2000 days of validity of the orbit. The results are shown in Figure 5 for the Fortran environment.

Note that since (i) the timescales and relativistic scaling are not identical (MOC has TDB and TDB-compatible coordinates, SOGAR being a DPAC software works with TCB and TCB-compatible quantities) and (ii) one uses also the orbit of the Earth from INPOP10e, the comparisons of both Java and Fortran codes were also an opportunity to validate these additional aspects of the implementations, and in fact a small bug was found in the Fortran library and fixed.

The results of comparisons were fully satisfactory and validated both Java and Fortran implementations. The residuals at a sub-metre level demonstrate only numerical agreement, and should not be mistaken for the absolute knowledge of where Gaia will be at a specific time. The actual uncertainty asked by DPAC to MOC is that Gaia should not depart from the predicted orbit by more than 7000 km. This number is 0.1 of the radius of Jupiter, meaning that the direction of Jupiter from Gaia is known within about $2''$ against the stellar background (see also Sect. 9.2).

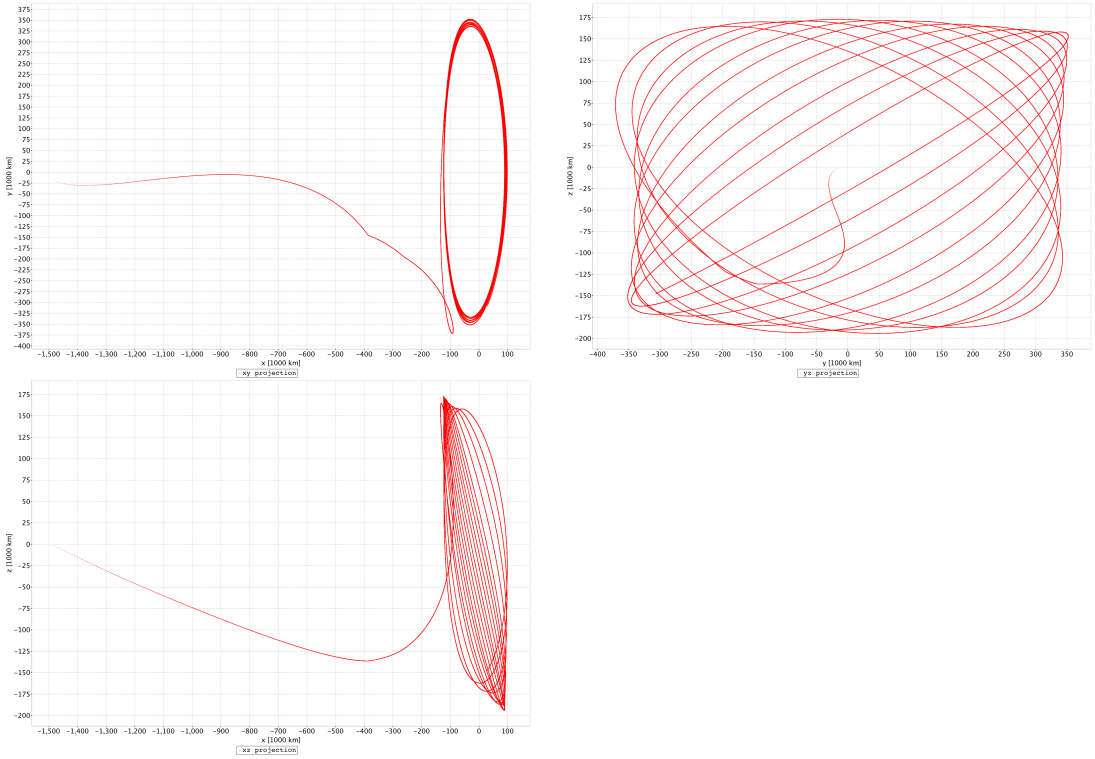


FIGURE 3: The delivered Gaia orbit in three projections XY, XZ and YZ with the X, Y and Z axes centred on and co-rotating with the L_2 point (so that the X axis is directed always from the Sun to L_2.

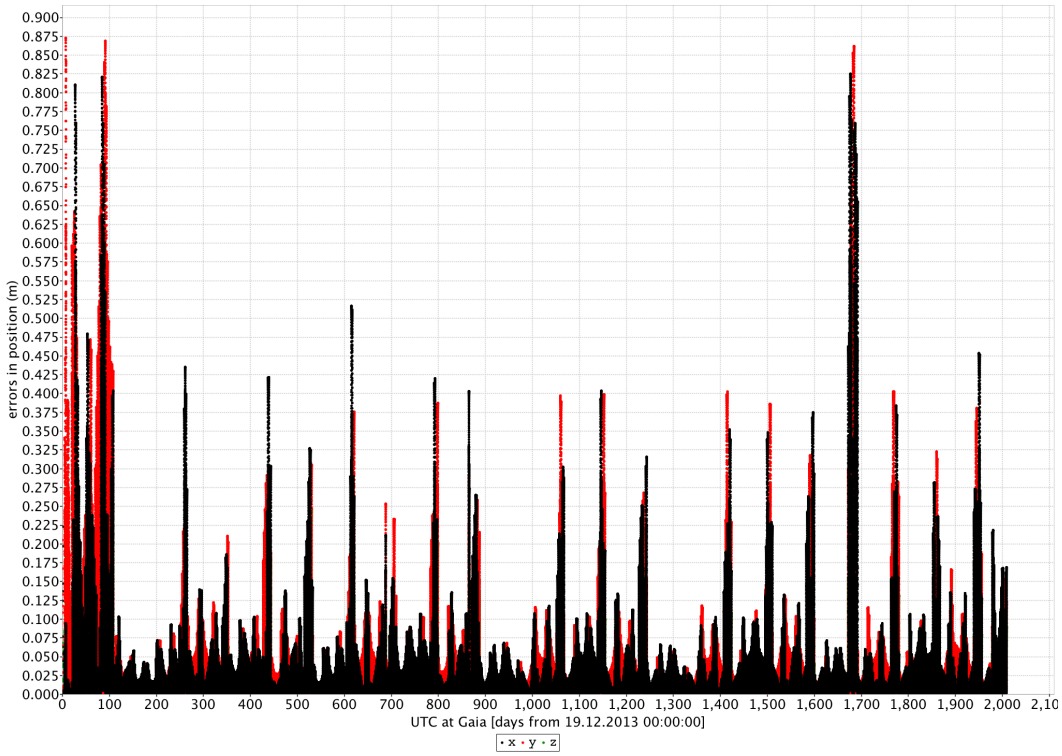


FIGURE 4: Verification of the orbit implementation in the Java code: absolute values of the residuals in Gaia position between the MOC orbit file and the gbin file as used in GaiaTools and in SOGAR/Java. Colours refers to the X, Y and Z coordinates in the co-rotating coordinates centred at L_2. The Z component is smaller and not visible in the plot.

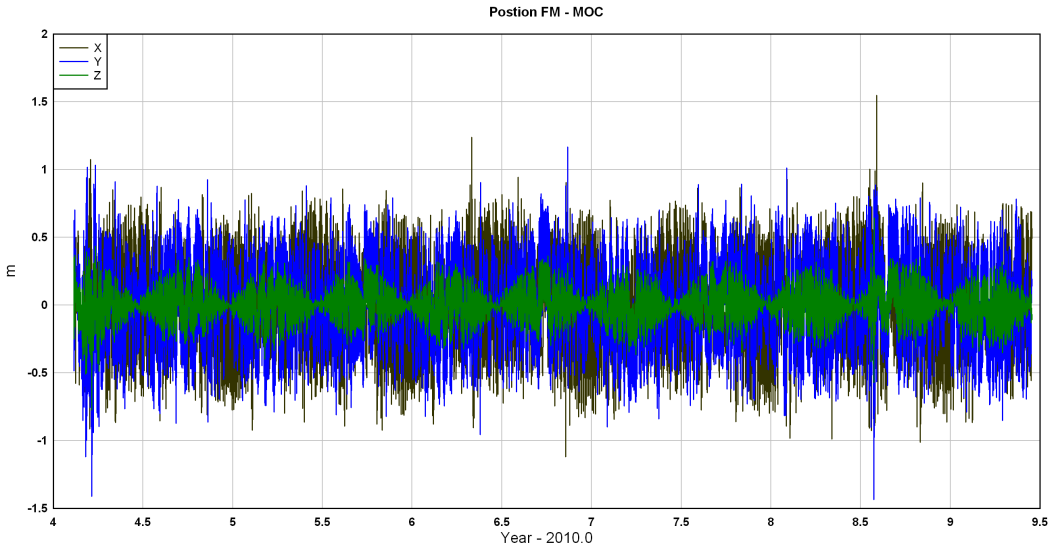


FIGURE 5: Verification of the orbit implementation in the Fortran code. Residuals in position between the MOC orbit file and the orbit access file used in SOGAR/Fortran.

4.3 Validation of the scanning law

Fundamentally there is no way to validate the MSL, since there is no other instance to compare. However its implementation has been checked extensively in 2013 by us and Lennart Lindegren in different ways. In particular specially for SOGAR needs L. Lindegren restructured the MSL implementation to improve the speed when using MSL on a grid of points for initial spin phases. Checks were conducted independently in Lund, Dresden and Nice. Initially we had a factor almost 100 between the runtime of SOGAR with NSL037 and MSL (MSL being 100 times slower), a very worrying situation since the operational SOGAR would have to be run on MSL and the computational costs with slow MSL would be too high to allow for a reliable optimization. After the upgrade the MSL runs became even slightly quicker than those with NSL037 and fast enough to allow to work with an high-resolution grid of initial conditions.

The main tools used for the validation was again the comparison to the analytical approximation NSL037, which has identical implementation in Java and Fortran. This identity, to the last significant digit, has been thoroughly checked by FM and Ch. Ordénovic, either on the pointing directions, the quaternions or the Euler angles. The identity of the SOGAR implementations in Fortran and Java running on the analytical NSL is another demonstration. Then MSL and NSL have been compared for various initial conditions and the differences over the mission duration did not show anything troublesome: no long term drift and no offset larger than the expected level based on the level of approximation done in the analytical solution, etc. In this process we found that the possibility to set initial conditions for the two free parameters at a specified time did not work well initially and this was corrected by L. Lindegren in a subsequent GaiaTools version to full satisfaction. Finally during SOGAR rehearsals in October 2012, we compared the MSL as used by SOGAR from the GaiaTools to the generation of the attitude ephemeris provided by SOC to MOC based on our selection of initial conditions. This testing went much beyond the MSL and allowed to evidence few snags in the implementation of the Hermite interpolations and in the handling of timescales which were fixed with SOC. All that contributed very much to improve the overall quality of the system and helped to converge towards a common understanding by all the people involved in the chain from DPAC to MOC.

5 Conventions for the initial conditions of the scanning law

There are a few conventions for the initial conditions for the scanning law – the initial precession and spin phases – that should be mentioned here. The initial phases are specified as input parameters of the method `setRefNuOmega` of the Java class `ModifiedScanningLaw` instantiated without high-density areas. The reference epoch for which these initial phases are given is specified by the GPDB parameter `GaiaParam.Mission.REFERENCEEPOCH_SCANNINGLAW_TCB` set as `JD2456536.5 TCB` (1 September 2013 00:00:00 TCB).

The initial spin phase is given using the heliotropic origin as the zero phase, and not the as-

cending node of the scan plane with the reference plane (celestial equator or ecliptic). This is in agreement with all the implementations of the scanning laws in the Gaia Tool. The origin of the precession phase is the intersection of the precession cone with the ecliptic leading the sun (longitude of the nominal Sun plus $45°$). Again this is implemented in the relevant classes and not visible to the users. Both conventions are described in the documents concerning the Scanning Law (e.g. those cited in HS-003).

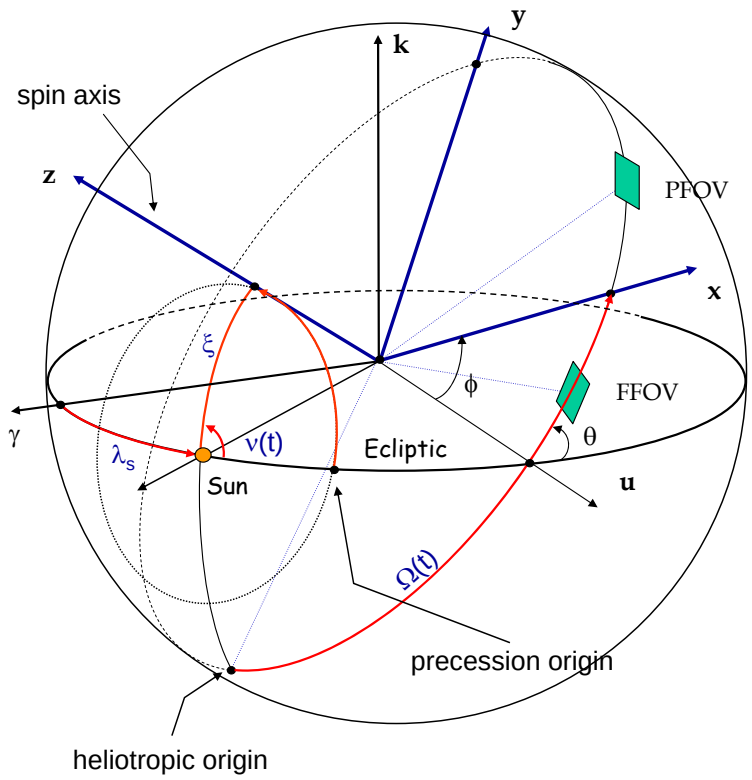


FIGURE 6: Diagram showing the four angles (in red) used in the formulation of the scanning law. The optimization deals only with the initial precession phase ν and the initial spin phase Ω. The initial values are referred to their respective origin at the reference time JD2456536.5 TCB.

6 Selection of good initial precession

6.1 The period of the search for the GAREQ-relevant observations

The search for the GAREQ observations were performed in the period between 8 July 2014 00:00:00 TCB and 10 May 2019 00:00:00 TCB. The duration corresponds to the 5 years of the nominal mission starting from the planned date of the IOCR (8 May 2013). The starting

date is selected from (partially wrong) idea that the nominal science operations start just after the IOCR with 28 days of EPSL followed by up to 34 days of NSL continuous with EPSL (no change of orientation between EPSL and that part of NSL is planned). In reality the EPSL starts already around 23 April 2014, so that the GAREQ-related optimization search could be started at a date two weeks earlier. However, it turns out that there are no GAREQ-relevant observations (of stars sufficiently close to Jupiter) from 25 May 2014 till 23 September 2014, because the ecliptic longitude of Jupiter is not compatible with the Gaia solar aspect angle and the planet cannot be seen by Gaia. This is true for any initial phases of the Scanning Law so that a change of the starting date for the search from 8 July 2014 to even 25 May 2014 does not change the results.

Another point that has been discussed and agreed with DPACE chair, Project Scientist and Project Coordinator is that no special observations of Jupiter (with actively adjusted initial precession and spin phases) are possible during the commissioning (before about 23 April 2014).

6.2 The selection criteria

As explained earlier we computed the s/n ratio for the quadrupole light deflection (also called the *efficiency factor* or the *figure of merit*) of each grid point of the initial conditions. The mathematical formulae used in SOGAR can be found in Mignard et al. (2014). Good initial conditions are not just that producing the largest figure of merit, although it should be among the largest. In preparing this recommendation we attempted to weigh several considerations to produce a good choice with the best chances of achieving the science objective. A list of criteria that were taken into account is as follows:

C1: Large cumulated s/n ratio for quadrupole deflection of light

The figure of merit must belong to the largest seen among all the grid points. Although this is not strictly quantified as the last decile or percentile, an histogram of all the values shows clearly that the interesting values belong to the extreme tails of the distribution, typically $\sim 5\sigma$ above the mean (Figure 7). In fact it is this feature which makes the optimization necessary and difficult, since picking initial conditions from another consideration will lead (in general) to nothing interesting for the relativity test. The vast majority of the grid points are uninteresting in this respect.

C2: Large area of good s/n ratios

We don't want to have a point isolated in a sharp spike among an ocean of low values. This would be too sensitive to the perfect implementation of the SL, to errors of the predicted Gaia orbit, and to the assumptions made in the software(see Sect. 9). Therefore we started the selection by identifying areas in the maps where large values concentrate, omitting possible larger values, which are too isolated.

C3: Solution good for all noise model

We have several noise models (Section 3.1), hoping that one of them is a good representation of the observation conditions close to Jupiter. The truth will be only known after the first few crossings of Jupiter seen by Gaia. Therefore to give us the best chances to carry out accurate astrometric measurements close to the Jupiter disk we try to select good areas which are common to the different noise models.

C4: Solution good also with a cropped field

We have also introduced a cropped field of view with transverse (AC) size 70% of the physical size to anticipate deviation of the true scan from the ideal mathematical solution, in order to increase the probability to have Jupiter in the FOV. We attempted to select good initial conditions that remain good even with this reduced FOV.

C5: Solution insensitive to a change of the scan rate

Fundamentally the optimization of the precession is normally not too sensitive to the adopted scan rate. However at the time the choice for the initial precession phase must be done, the precise actual scan rate is not known. Runs were done with the nominal value deduced from the designed focal length. It has been shown during the development phase, that with scan rates within 1% of the reference value the favourable grid points are stable in precession and shifts in scan phase (Mignard and Ordenovic, 2013). Our choice should be stable against a potential deviation of the scan rate of that size. This is a serious issue and it is further investigated in Sect. 9.

C6: Differential and global analysis

With Gaia observations there are two ways of exploiting the observations of stars close to Jupiter. The *differential method* needs to have sequences of consecutive observations of the same star field(s) over few hours, with Jupiter moving during this period. The same star(s) is (are) seen affected or not by the quadrupole deflection and shares more or less a common attitude error. The *global method* seeks the quadrupole deflection parameter from the astrometric global iterative solution (AGIS) as a general global parameter as available in the framework of the Generic Global Update (GGU). The same star is seen ~ 65 times during the mission and only once or twice with Jupiter close by. Sequences are less important, but closeness to Jupiter at least once is essential. In our selection we tried to find conditions and stars useful for both methods.

C7: Good observations early in the mission

As the mission will advance in time the CCD efficiency may degrade, some may even become unusable. As any space mission the risk in space is non-zero and while we have a nominal duration of 5 years, we have better probability to catch earlier events than those occurring late in the mission. This would favour initial conditions leading to events during the first two years relatively to later events.

However the sky motion of Jupiter during the mission does not offer that liberty. Jupiter is close to the galactic plane with the denser star fields around in 2013 and early 2014 and again 5 years later when the planet has moved to the other node of its orbit with the Galactic plane. It happens that the node of 2018 is almost coincident with the galactic centre and the number of close approaches with stars increases dramatically. Therefore in practice most of the events producing a large value of the merit function will be towards the end of the nominal mission.

C8: Several good stars/observations

Given the uncertainties of real operations of Gaia (e.g. the partially unpredictable dead time) it is would be too risky an option to select a point dominated by one or a few observations of just one star to be performed during a few hours. A good selection must rest on several good observations at different epochs. If one is missed, one still has the chance for the next.

C9: Not all observations in crowded areas

Events within crowded fields should be avoided, or at least considered with lower priorities. However as mentioned above the presence of Jupiter around the galactic centre in late 2018 and early 2019 is an advantage for the number of close encounters with stars, so potentially the best period for the number of events, but the price to pay are observations in crowded fields. In our selection, if a good grid point is too much dominated by a single event in 2019, it is avoided. This is a precaution, since Gaia can really observe in mild crowded fields. Furthermore, we are focusing on bright stars ($G < 15$) whose observations are normally not too much affected by surrounding faint stars.

C10: Observation of stars close to Jupiter before the main events

In case the interesting events do not arise close to the mission beginning, it would be useful if the selected grid point allowed several occurrences of Jupiter crossings before the first valuable event, with stars not to far, say at few Jupiter radii. This will be an opportunity to evaluate the astrometric performance and learn a little about this particular observing condition.

C11: No-problem stars

Gaia observes stars, not Jupiter. The astrometric signal comes from the stars, not from the planet. So one needs to select observations with *no-problem stars*: single stars, with position confirmed with sky images, small proper motions are better for the differential method, bright stars but not too bright to avert the possible gate calibration issue. So when good grid points are identified, they are eventually confirmed only after the stars contributing to the signal are looked at in detail with the CDS tools and qualified for the job.

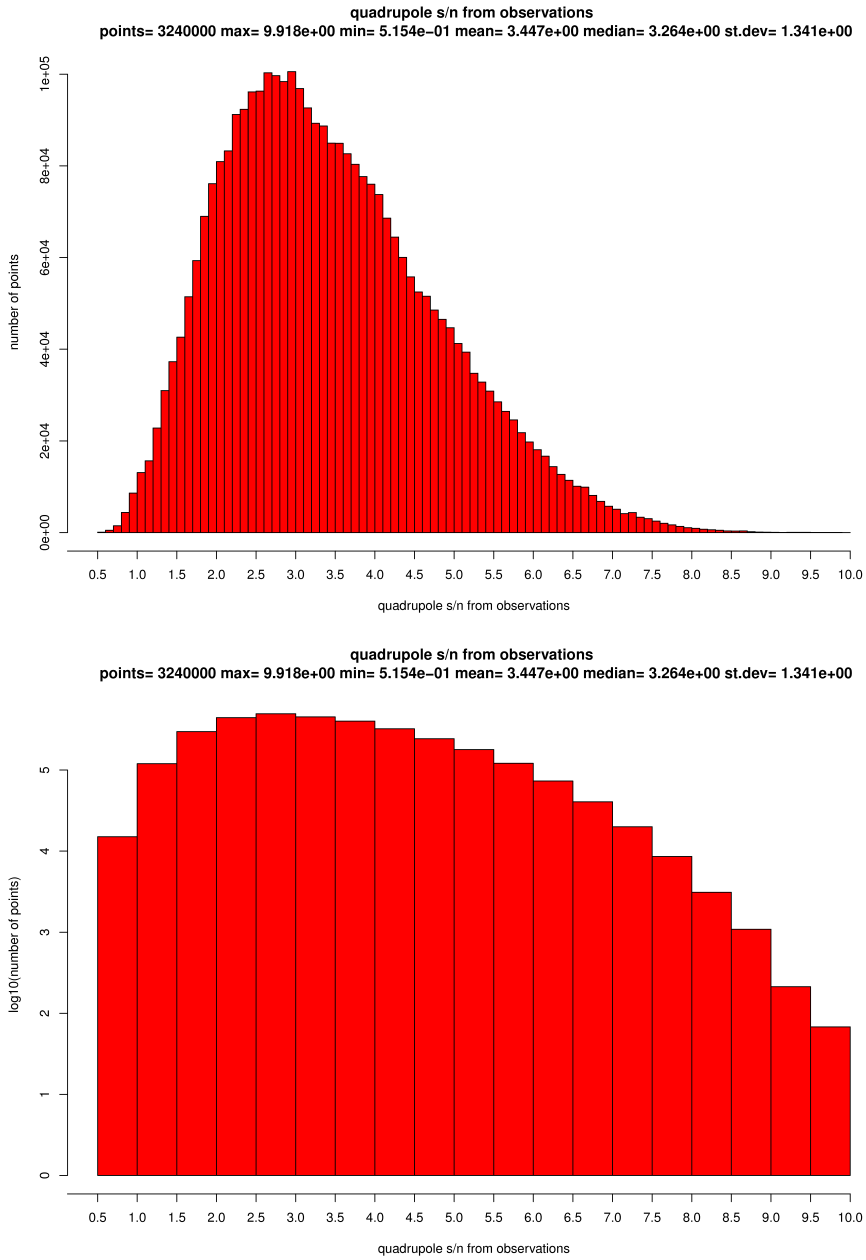


FIGURE 7: Distribution of the values of the s/n ratio for the individual points on the $0.2^\circ \times 0.2^\circ$ grid in the initial precession and spin phases (a total of $(360/0.2)^2 = 3240000$ points). The histogram here is shown for the noise model N_3, in linear (upper pane) and logarithmic (lower pane) scales. A random choice of the initial conditions would end up with something in the range 2 to 4, while it is possible to select a good one on the rightmost tail, as large as 9.9, about 5σ away from the mean. The situation is similar for the other two noise models.

Noise model	AC extension	
	100%	70%
N_1	Figure 8	Figure 9
N_2	Figure 10	Figure 11
N_3	Figure 12	Figure 13

TABLE 2: Figures with the colour-coded maps of the s/n ratio as function of initial precession and spin phases corresponding to the three noise models and two AC extensions of the FOV considered as available for GAREQ observations.

6.3 Selection of the potentially good areas

The process of selection starts with computing the values of the s/n ratio for the quadrupole effect for a sufficiently fine grid for the initial precession and spin phases. Given the hardware readily available for the SOGAR team we decided to use the grid with a step of 0.2° in both angles, thus checking $(360/0.2)^2 = 3240000$ combinations of initial phases. This calculation was repeated six times: for 3 noise models – N_1, N_2 and N_3 – and two configurations for the AC extension of the FOVs – for the full AC extension and with the AC extension of 70%. The s/n values are represented as colour-coded maps and shown on Figure 8–13. Table 2 can be used to access these Figures. Considering the criteria formulated in Section 6.2 one can find a few regions in two angles that *potentially* satisfy criteria C1 – C4. These are shown on Figure 14. Four of regions of interest - 1, 2, 3a and 3b – were investigated using finer grids with a step of 0.02° in both angles. These fine grids were again computed in six versions to check the criteria C1 – C4. The fine-grid maps for the finally selected region 2 are shown on Figures 15–20 and summarized in Table 3. For region 4 several points were checked manually against criteria C1 – C11. The results of this analysis is given in Section 6.4.

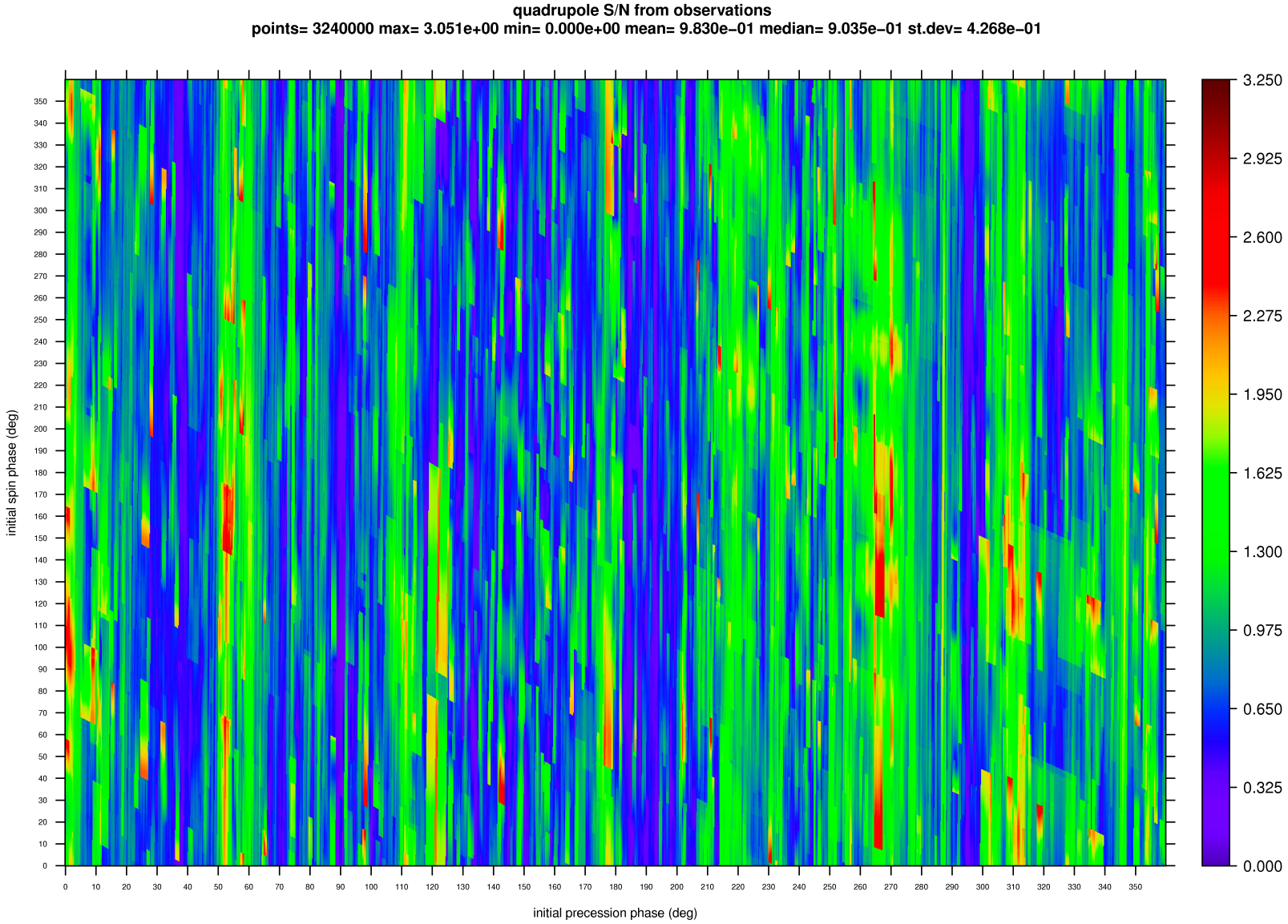


FIGURE 8: The colour-coded map of the s/n ratio on the $0.2^\circ \times 0.2^\circ$ grid of initial precession and spin phases using the noise model N_1 and full AC extension of the FOVs.

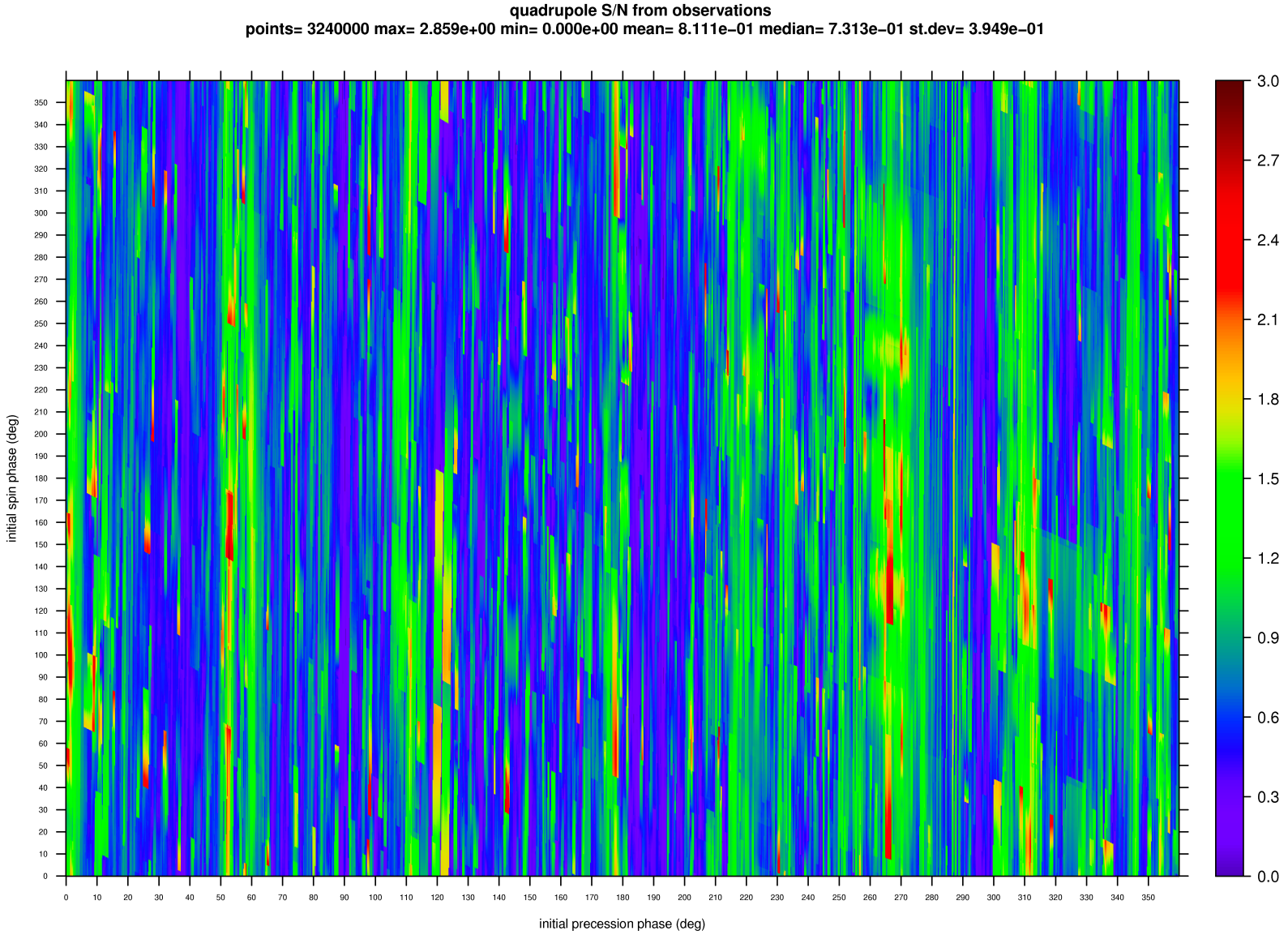


FIGURE 9: The colour-coded map of the s/n ratio on the $0.2^\circ \times 0.2^\circ$ grid of initial precession and spin phases using the noise model N_1 and the AC extension of the FOVs reduced to 70%.

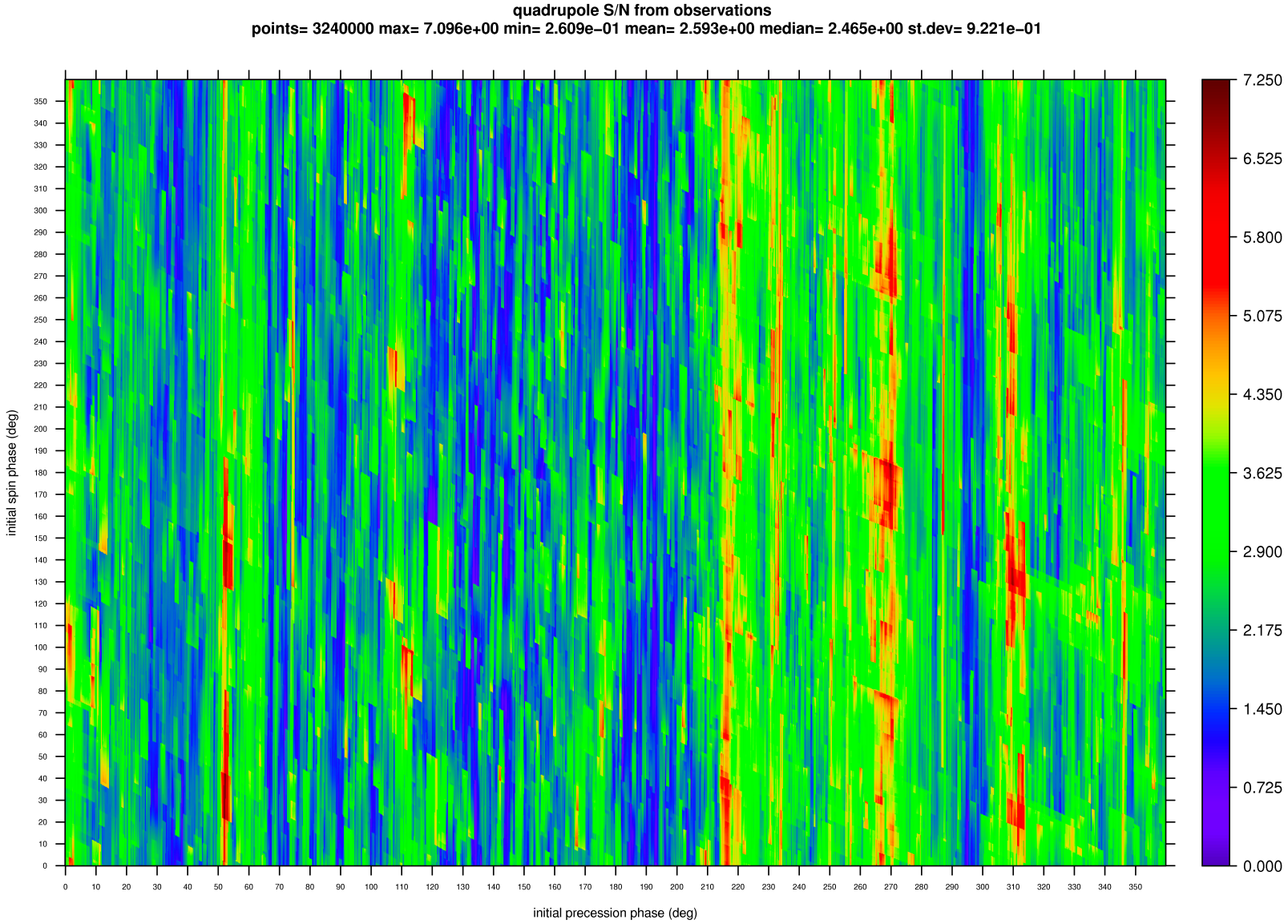


FIGURE 10: The colour-coded map of the s/n ratio on the $0.2^\circ \times 0.2^\circ$ grid of initial precession and spin phases using the noise model N_2 and full AC extension of the FOVs.

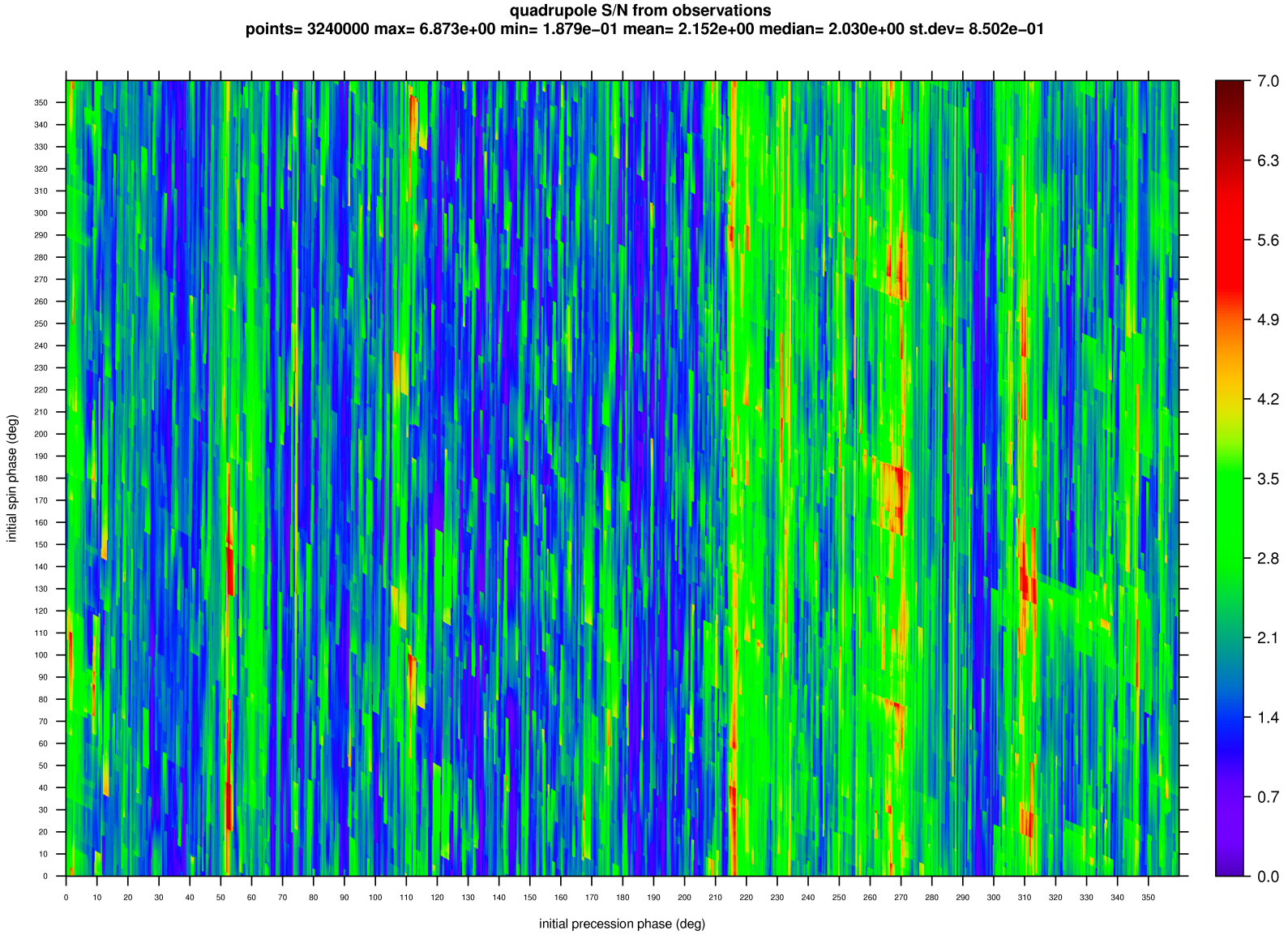


FIGURE 11: The colour-coded map of the s/n ratio on the $0.2^\circ \times 0.2^\circ$ grid of initial precession and spin phases using the noise model N_2 and the AC extension of the FOVs reduced to 70%.

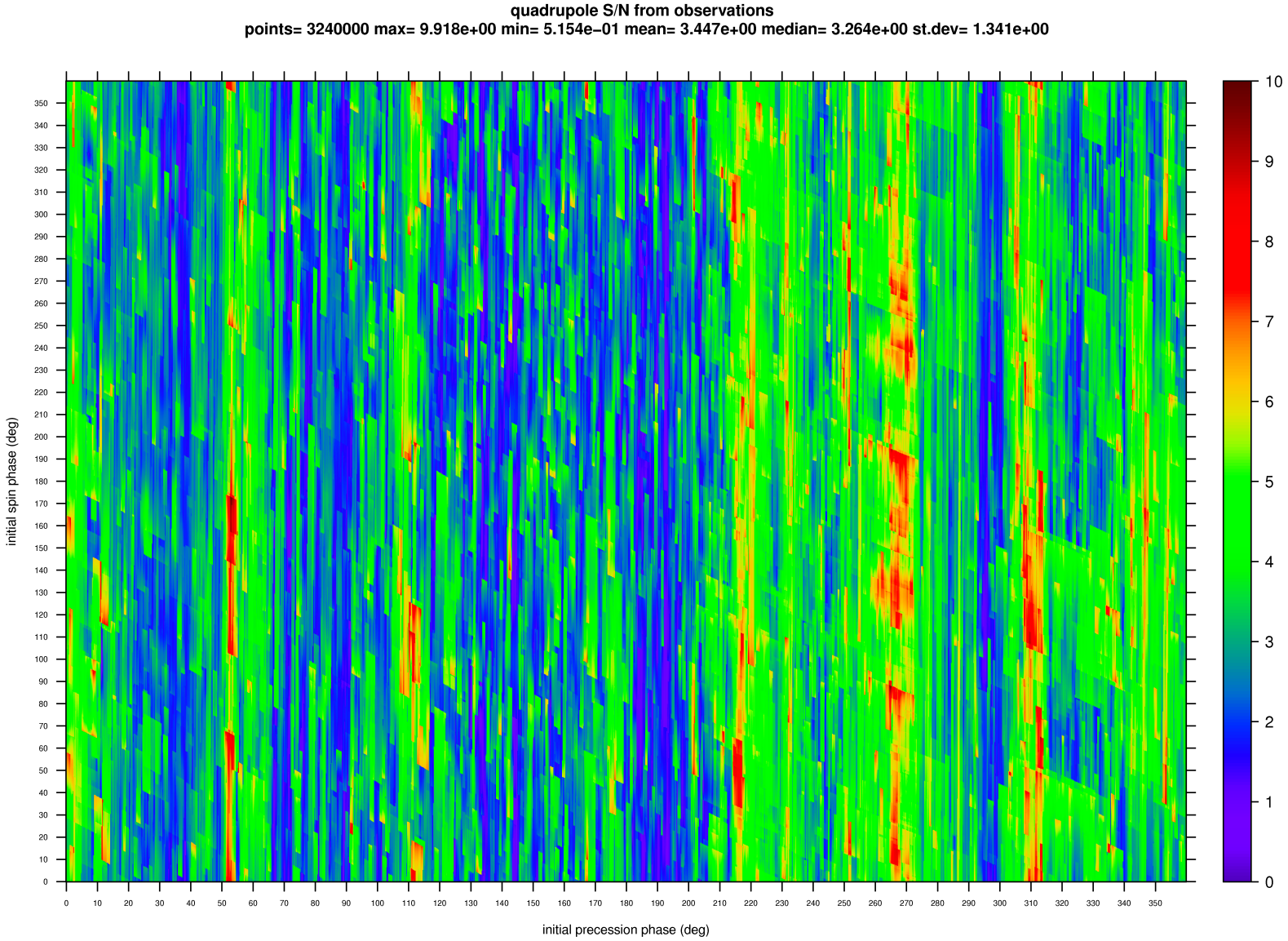


FIGURE 12: The colour-coded map of the s/n ratio on the $0.2^\circ \times 0.2^\circ$ grid of initial precession and spin phases using the noise model N_3 and full AC extension of the FOVs.

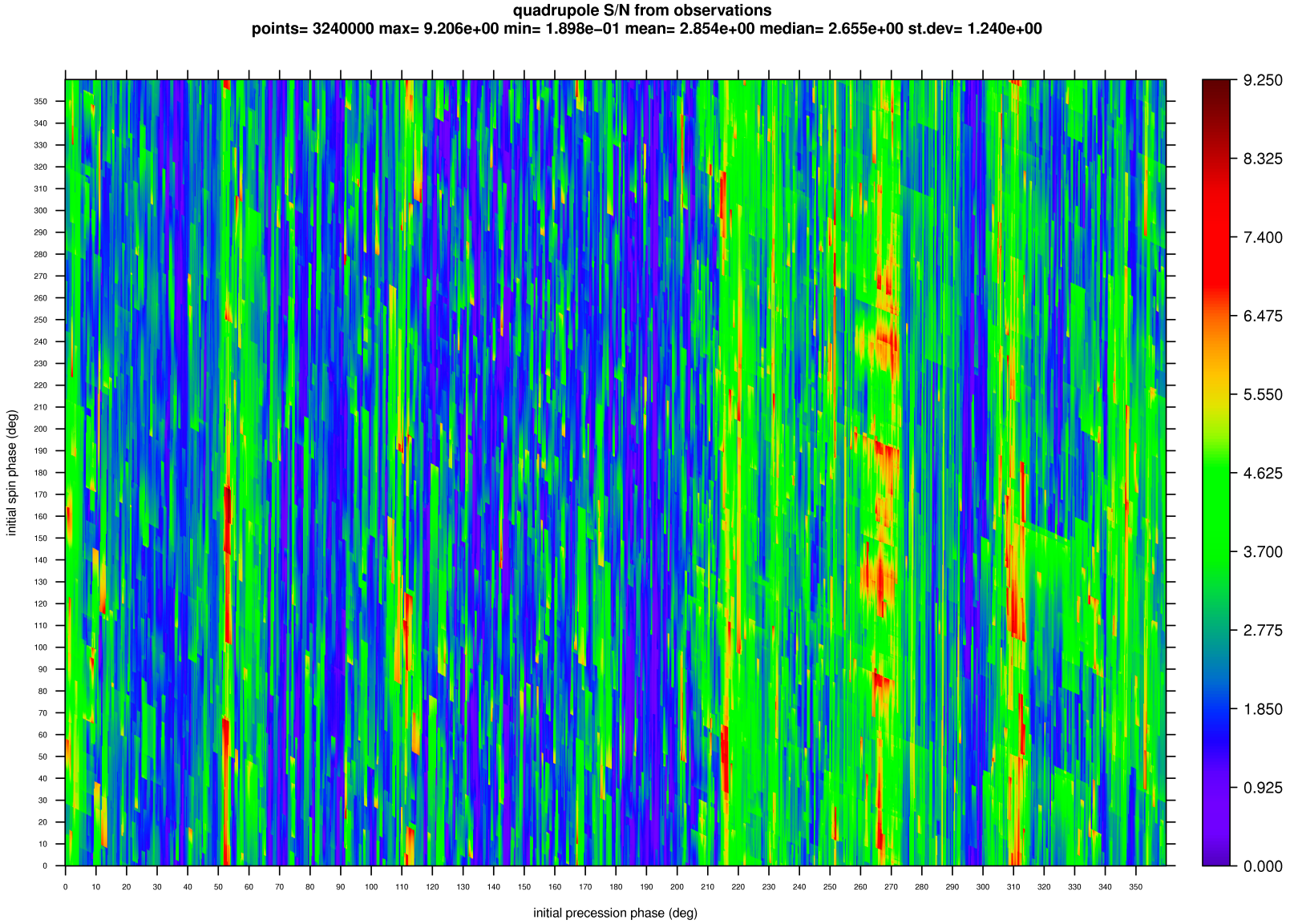


FIGURE 13: The colour-coded map of the s/n ratio on the $0.2° \times 0.2°$ grid of initial precession and spin phases using the noise model N_2 and the AC extension of the FOVs reduced to 70%.

Noise model	AC extension	
	100%	70%
N_1	Figure 15	Figure 16
N_2	Figure 17	Figure 18
N_3	Figure 19	Figure 20

TABLE 3: Figures with the colour-coded maps of the s/n ratio in the Region 2 as function of initial precession and spin phases corresponding to the three noise models and two AC extensions of the FOV considered as available for GAREQ observations.

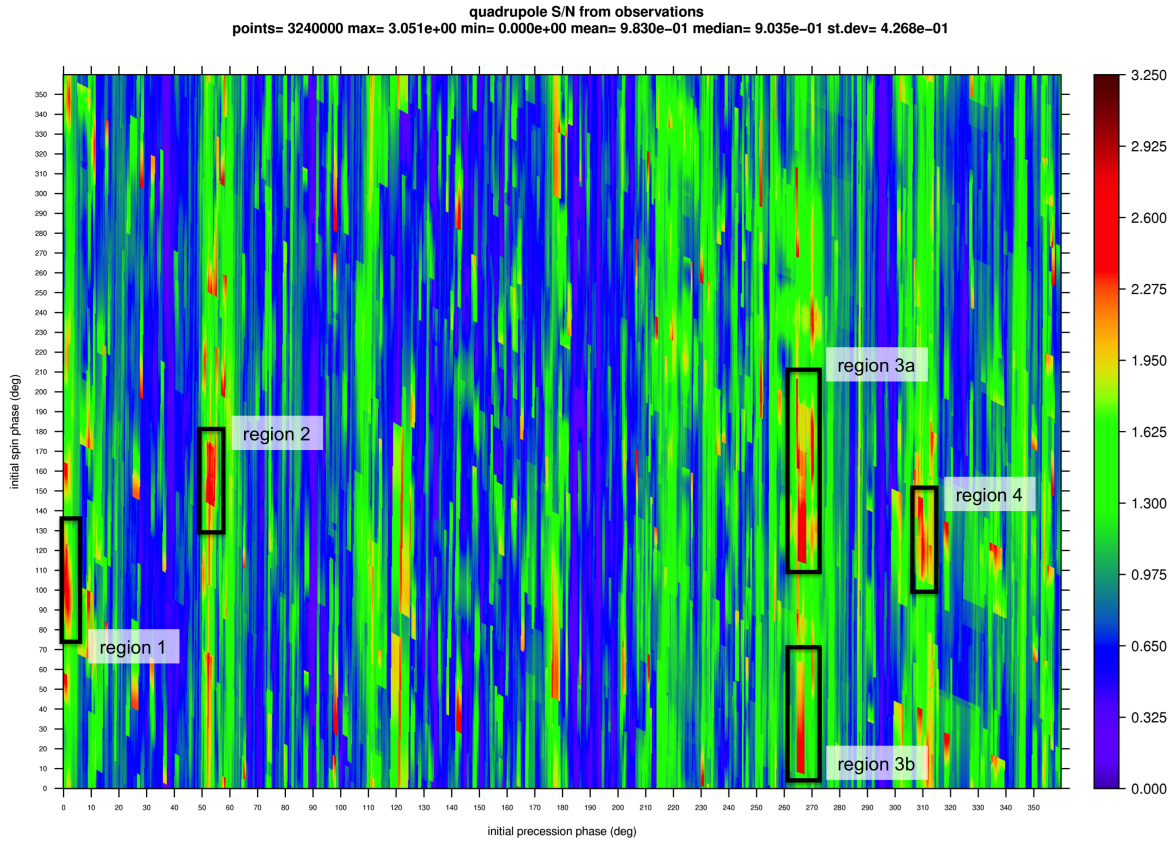


FIGURE 14: Regions of interest in the colour-coded map of the s/n ratio for the quadrupole light deflection to be explored with higher-resolution grid.

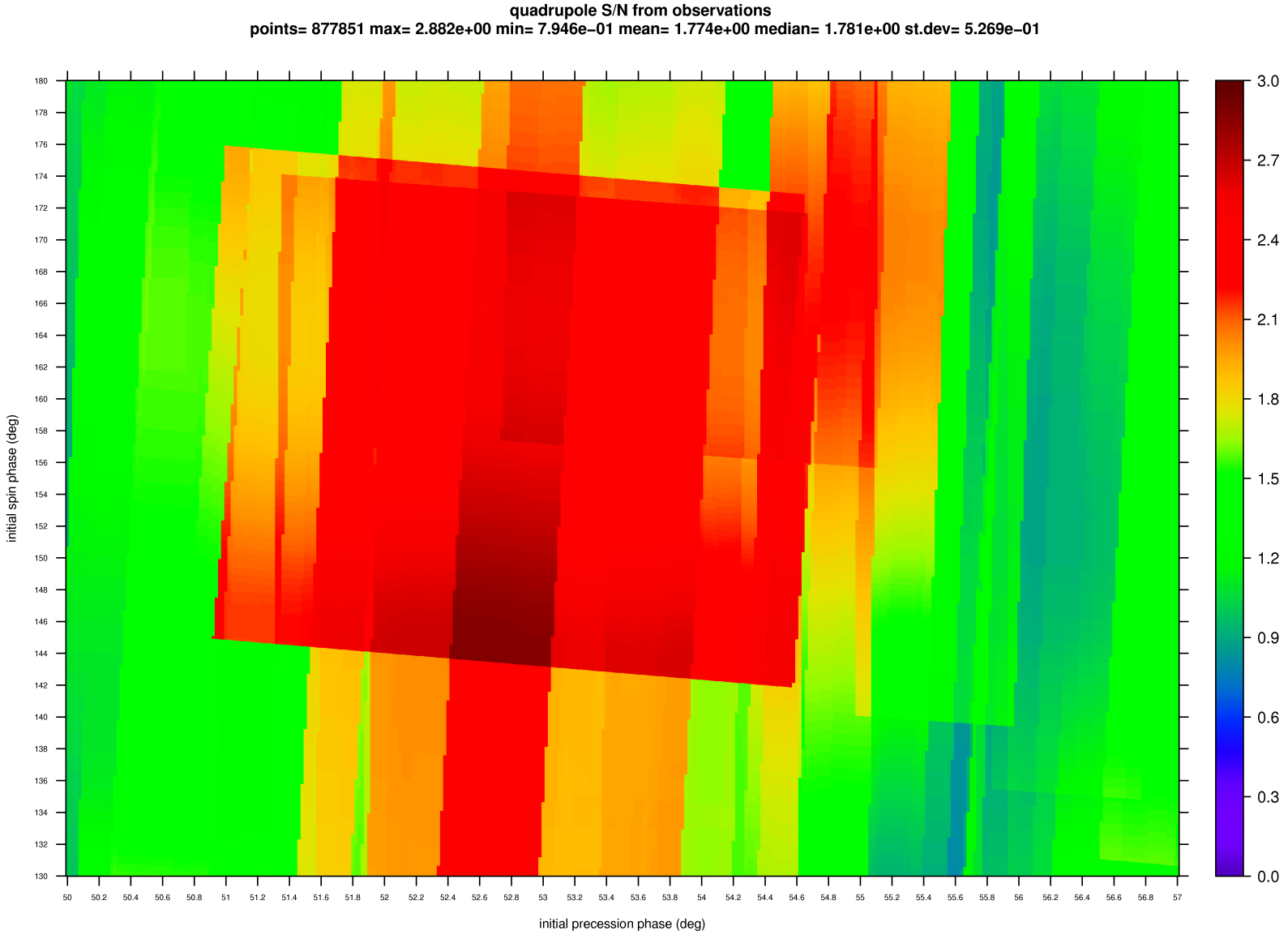


FIGURE 15: The colour-coded map of the s/n ratio on the $0.02^\circ \times 0.02^\circ$ grid of initial precession and spin phases in region 2 using the noise model N_1 and full AC extension of the FOVs.

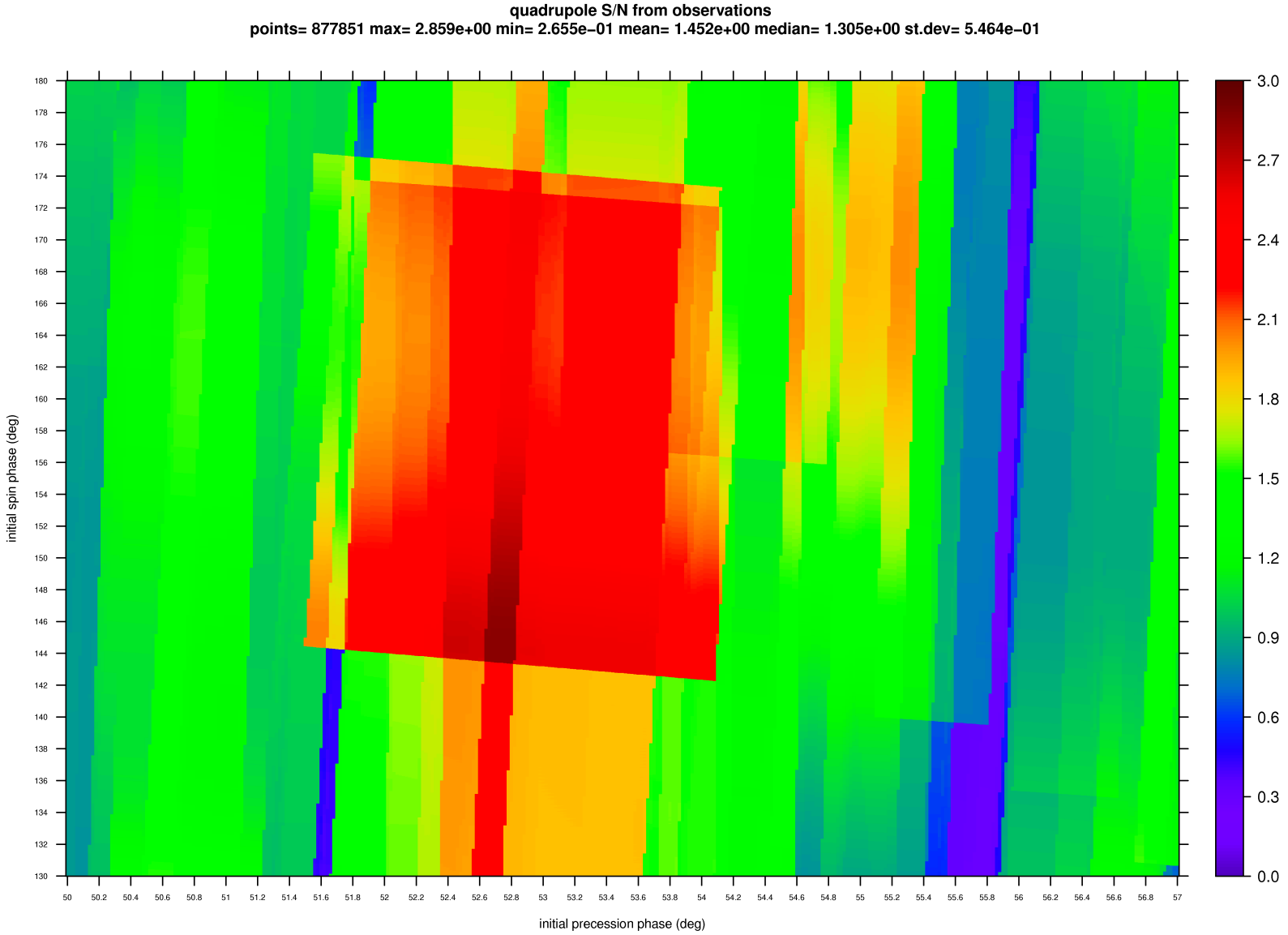


FIGURE 16: The colour-coded map of the s/n ratio on the $0.02^\circ \times 0.02^\circ$ grid of initial precession and spin phases in region 2 using the noise model N_1 and the AC extension of the FOVs reduced to 70%.

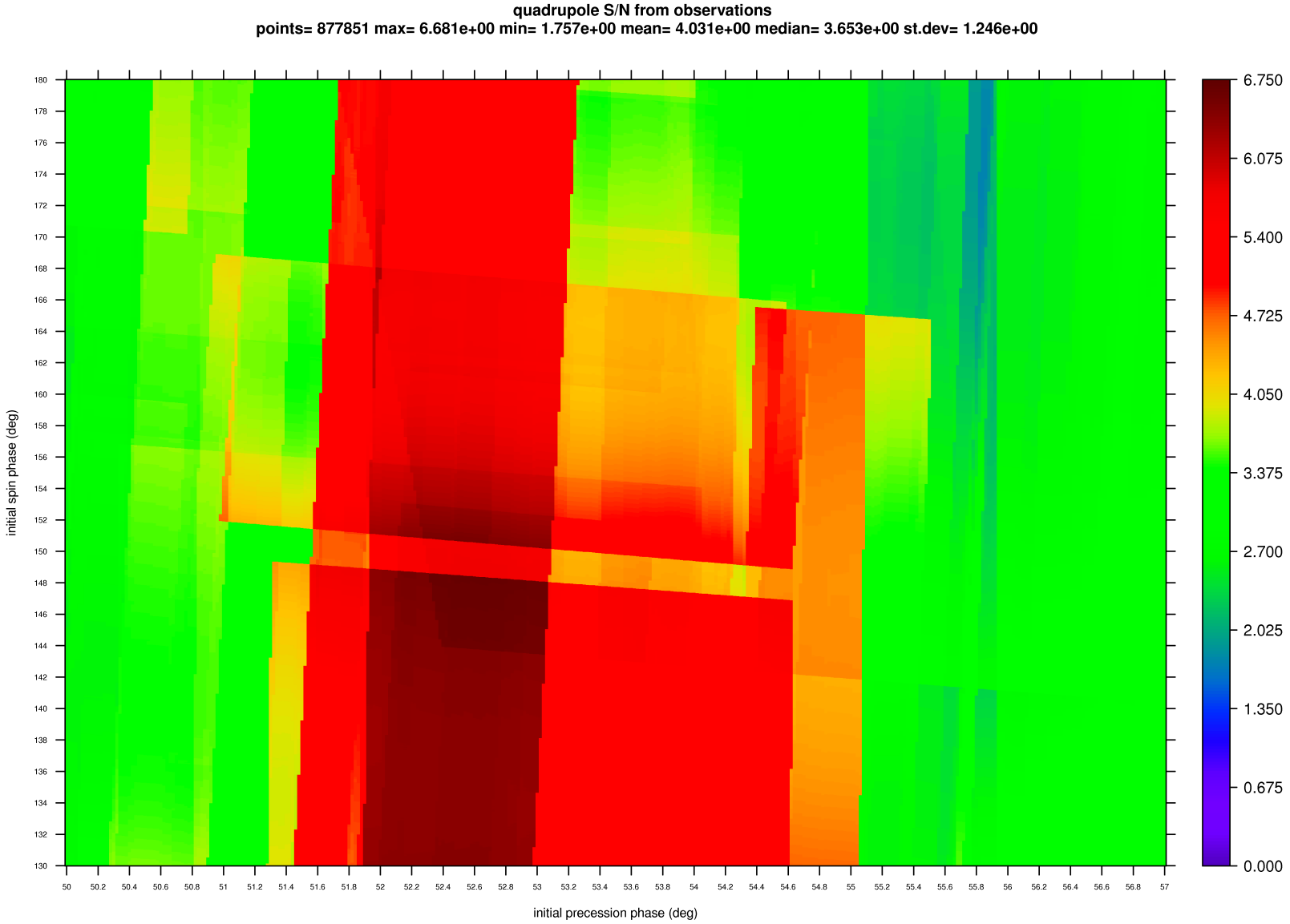


FIGURE 17: The colour-coded map of the s/n ratio on the $0.02^\circ \times 0.02^\circ$ grid of initial precession and spin phases in region 2 using the noise model N_2 and full AC extension of the FOVs.

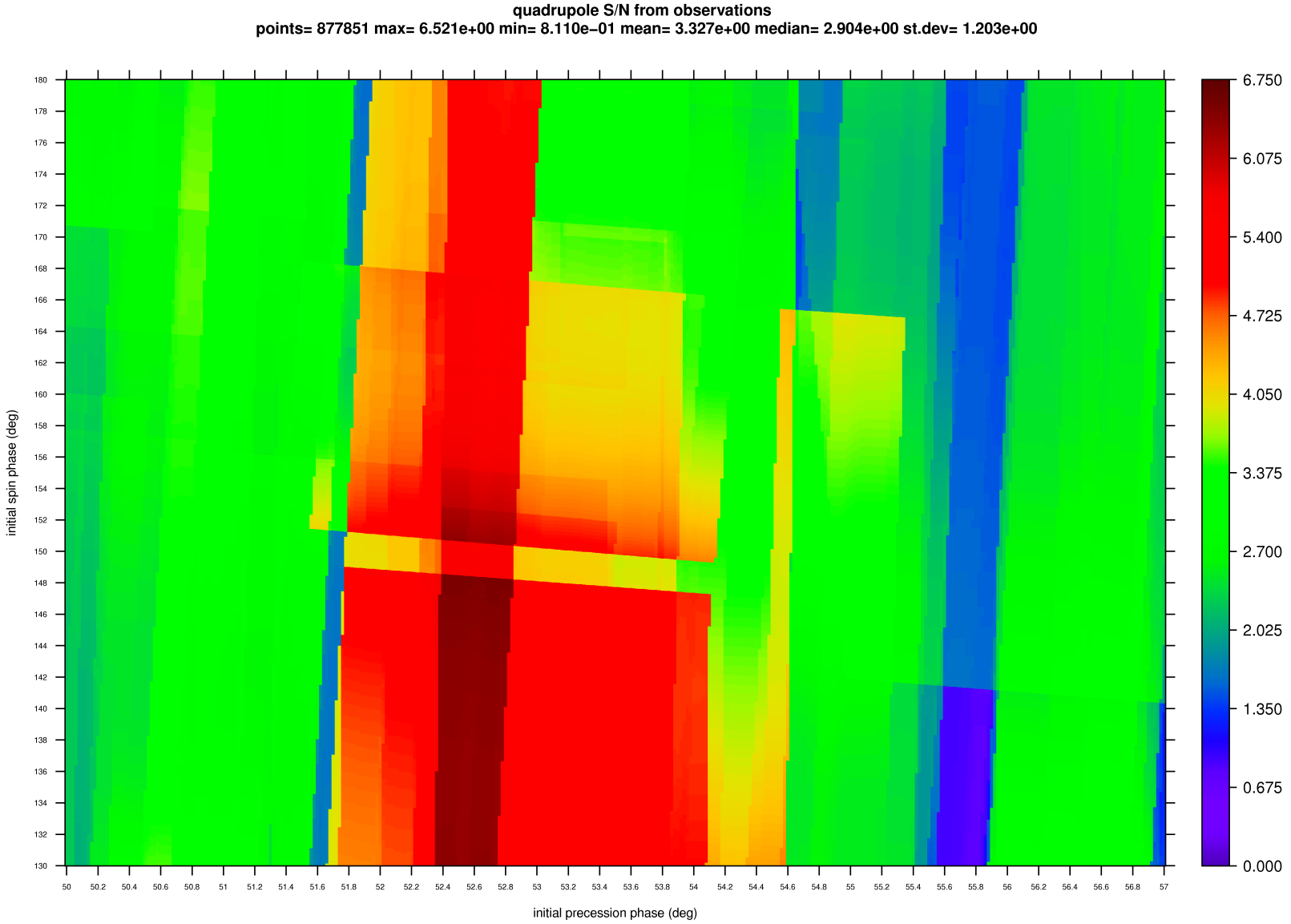


FIGURE 18: The colour-coded map of the s/n ratio on the $0.02^\circ \times 0.02^\circ$ grid of initial precession and spin phases in region 2 using the noise model N_2 and the AC extension of the FOVs reduced to 70%.

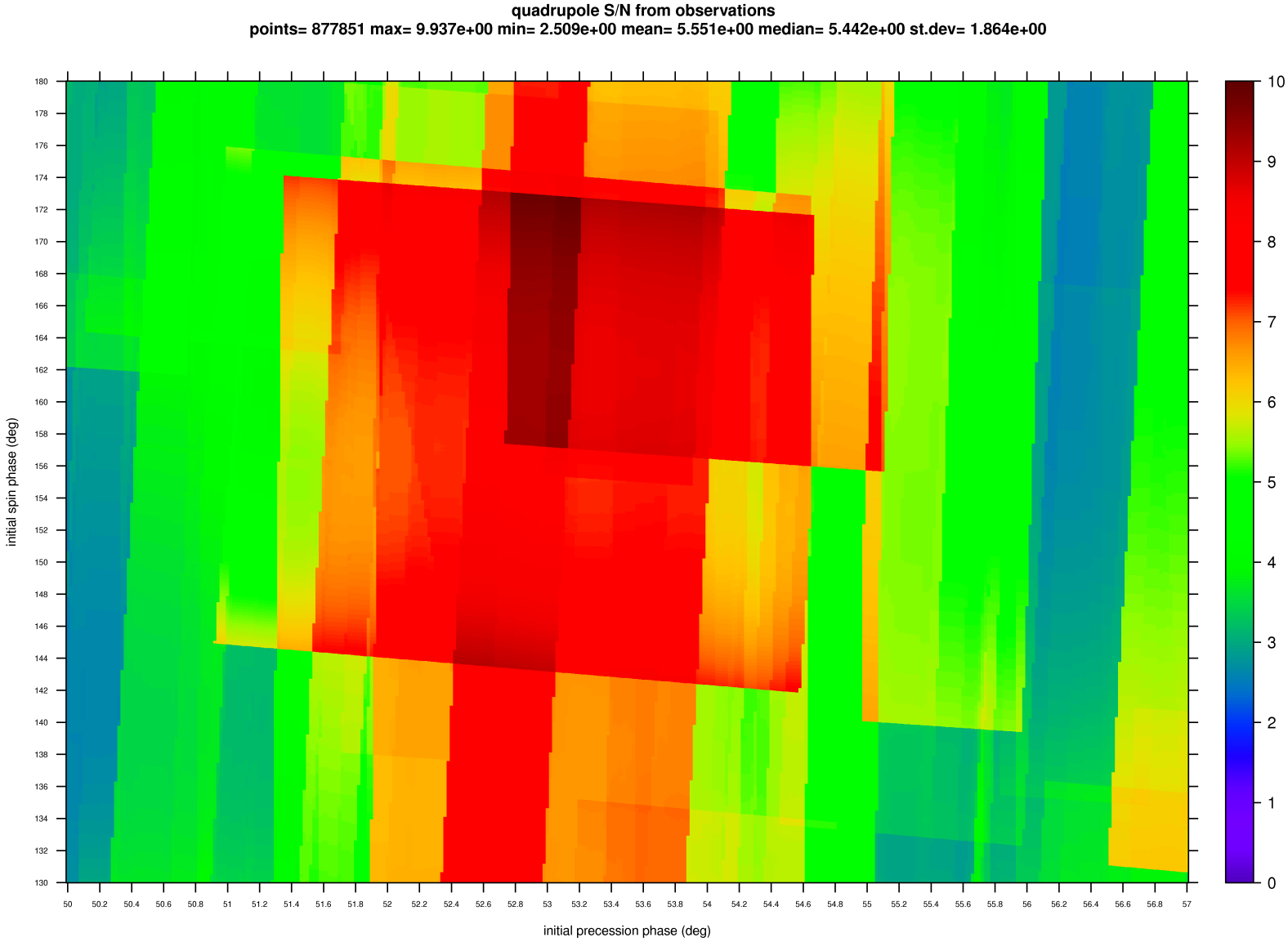


FIGURE 19: The colour-coded map of the s/n ratio on the $0.02^\circ \times 0.02^\circ$ grid of initial precession and spin phases in region 2 using the noise model N_3 and full AC extension of the FOVs.

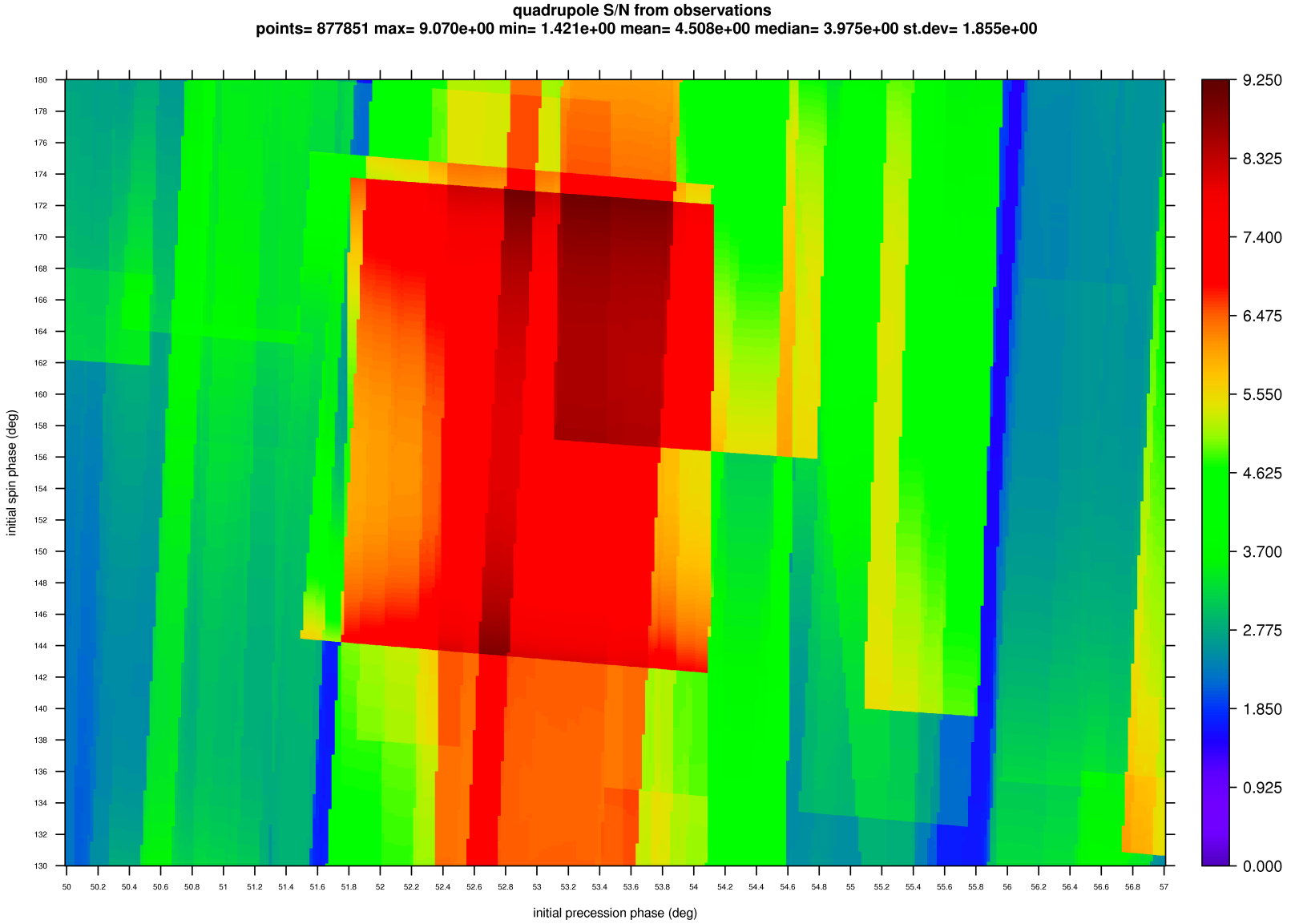


FIGURE 20: The colour-coded map of the s/n ratio on the $0.02^\circ \times 0.02^\circ$ grid of initial precession and spin phases in region 2 using the noise model N_2 and the AC extension of the FOVs reduced to 70%.

6.4 Ranking of the candidate solutions

In each region of interest at least one grid point is selected in each of these areas and ranked against the 11 criteria described in Section 6.2.Ranks for each of the criteria are denoted as A, B, C, where A means the criterion is fulfilled, C when the grid point does not meet at all the requirement, and B for an intermediate situation. To achieve this ranking the colour-maps for 3 different noise models and 2 different AC extensions have been closely examined (both global ones and the high-resolution maps restricted to some regions of interest). This was used mainly for criteria C1 to C4. Then for the best selected point in each area of interest, we look at all the stars which were seen in the vicinity of Jupiter up to 6 Jupiter radii and ranked criteria C6 to C9. Criterion C10 was eventually ranked for the stars which passed all the other tests and producing a large s/n value. Then criterion C5 was checked only for the final selection (see Section 9.3), since the corresponding check requires extensive computations. The results are summarized in Table 4, where the last line gives the overall standing.

Criteria	Explored region as on Figure 14				
Section 6.2	1	2	3a	3b	4
C1	C	A	A	A	B
C2	-	A	A	A	B
C3	-	A	B	C	B
C4	-	A	A	B	A
C5	-	B	-	-	-
C6	-	A	B	B	A
C7	-	B	C	A	A
C8	-	A	B	C	B
C9	-	A-	A	A	-
C10	-	A	B	A	A
C11	-	A	B	C	C
Ranking	-	1	2	-	-

TABLE 4: Ranking according to our selection criteria of the candidate solutions explored in detail.

Here are some notes on the ranking for the selected regions:

Region 1:

C1: The area is unstable with the noise model. It was initially selected based on the model N_1, but then it was quickly realized that for the other two models the hot spot is not stable enough. No further investigation of this region was undertaken.

Region 2:

C5: Moderately stable with change in scan rate (see Section 9.3).

C7: The first valuable event is in February 2017.

C9: One star appears in a crowded field when looked with the 2MASS catalogue.

Region 3a:

C6: No good sequence for the differential solution

C7: All events, except two too bright stars, happen in 2019

C11: The two main stars are bright (magnitudes 10.4 and 10.8).

Region 3b:

C1: The star that gives about 80% of the s/n value is observed very close to Jupiter (angular distance very close to $2''$). This is allowed by all considered models, but is too dangerous to rely upon.

C3: The best points are not stable with a change in noise model

C6: No good sequences for the differential solution.

C8: 80% of the s/n built up on a single bright star of magnitude 10.4. The star is observed during 7 hours of observations. It seems to be too dangerous, since a break in observations during these 7 hours almost completely destroys the GAREQ.

C11: The relevant star is too bright (magnitude 10.4 meaning that the third brightest/smallest gate should be used).

Region 4:

C1: The s/n is significantly below the reachable maximum.

C8: There is only one star giving s/n ratio > 1 for the model N_1.

C11: The main star is too bright (magnitude 10.3 meaning that the third brightest/smallest gate should be used) and very close to Jupiter (angular distance $\sim 2''$)

6.5 Check with ALADIN on few prominent stars

Finally for the best candidates for the initial precession and spin phases, individual observations were investigated and the sky environments for the most important stars were checked using the CDS tools (ALADIN, SIMBAD, etc.). Figures 21–23 show the ALADIN screenshots for the sky environments of the three most important stars for the finally selected point as given in Section 6.6 (see Section 7 and Appendix A for the individual observations for this point). The ALADIN screenshots show the sky environments in optical (DSS) and infrared (2MASS) wavebands. Gaia should see a mixture of these two images.

6.6 Recommendation of a precession initial value

Based on the above ranking of the potentially acceptable choices, one choice, area 2, stands clearly above all the others. Our recommendation is then to set up the Nominal Scanning Law with the initial precession at reference time to $\nu_0 = 52.66°$. The initial spin phase was selected using the GPDB value of the spin rate: 59.964185780301335 arcsec/s in TCB. With a spin rate of 60 arcsec/s in TCB, the consistent best initial spin phase is found at $\Omega_0 = 353.60°$. Thus, as planned the value of the initial spin phase is provisional and will be updated as soon as the in-flight scan rate is known (currently planned for L+10 weeks).

parameter	notations	value	units
precession phase	ν_0	52.66	degrees
spin phase	Ω_0	146.00	degrees

TABLE 5: Recommended initial conditions. The initial spin phase is still provisional and is only meaningful with the adopted GPDB scan-rate value of 59.964185780301335 arcsec/s.



FIGURE 21: Screenshot of the ALADIN windows with the sky environment of the source with coordinates $\alpha = 201.4053°$, $\delta = -7.3830°$. The left pane shows coloured DSS view and the right one shows coloured 2MASS data.



FIGURE 22: Screenshot of the ALADIN windows with the sky environment of the source with coordinates $\alpha = 228.6469°$, $\delta = -17.2359°$. This star is TYC 6174-830-1. The left pane shows coloured DSS view and the right one shows coloured 2MASS data.

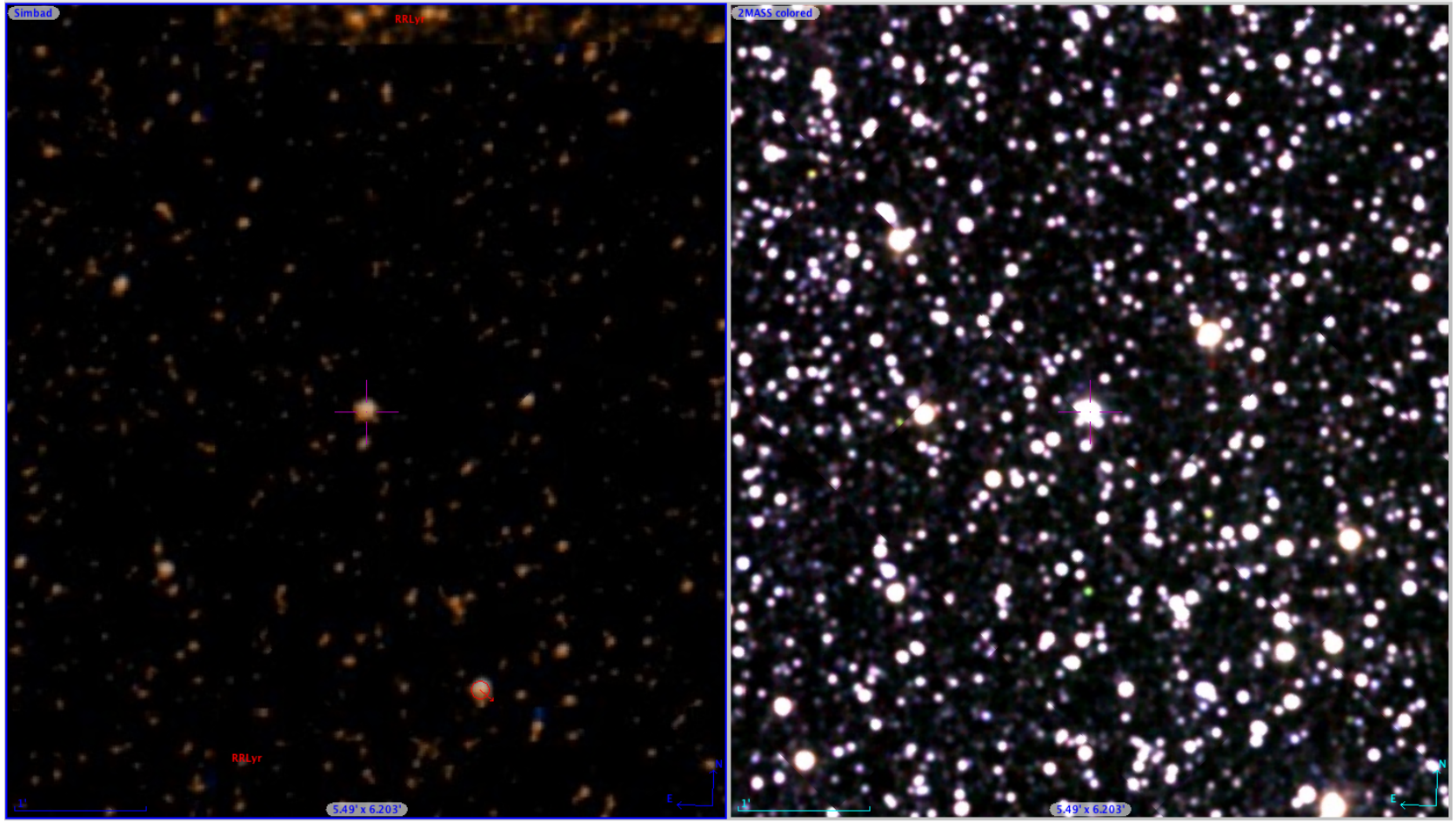


FIGURE 23: Screenshot of the ALADIN windows with the sky environment of the source with coordinates $\alpha = 263.6591°$, $\delta = -22.6800°$. The lower pane shows coloured DSS view and the upper one shows coloured 2MASS data.

7 Relevant observations for the recommended initial precession phase

We detail in this Section the top level GAREQ events whose cumulated values of the merit function contribute to more than 80% of the total detection capability. For each event and for each star contributing, one gives the star coordinates and magnitude, the crossing(s) times, the distance to Jupiter centre in Jupiter radii, the distance to Jupiter limb in arcsec, the s/n contribution for every crossings of this star happening just before or just after the closest approach to Jupiter. The circumstances of the three most important events are detailed in Table 6. One finds in the table the coordinates of the stars, the observation times, the distance from the centre of Jupiter and the efficiency of the detection expressed as s/n ratio. The geometry of the first event in February 2017 is shown in Figure 24 with the 9 observations plotted against Jupiter in the FoVRS frame and Jupiter oriented as it should be during this event. The first observation in Table 6 is located bottom-left. Figure 25 presents a close-up view for observations 4 and 5 over the quadrupole deflection field.

star	obs. no.	star α deg	star δ deg	mag	date days	dist Jup R_J	dist Jup arcsec	s/n N_1	s/n N_2	s/n N_3
1	1	201.4053	-7.3830	12.92	2609.7974	4.28	88.9	0.05	0.08	0.08
1	2	”	”	12.92	2609.8714	3.60	74.9	0.09	0.14	0.14
1	3	”	”	12.92	2610.0476	2.00	41.6	0.49	0.96	0.96
1	4	”	”	12.92	2610.1216	1.35	28.1	1.02	3.19	3.19
1	5	”	”	12.92	2610.3717	1.25	26.1	0.86	3.18	3.18
1	6	”	”	12.92	2610.5479	2.86	59.5	0.03	0.05	0.05
1	7	”	”	12.92	2610.6219	3.56	74.9	0.00	0.01	0.01
1	8	”	”	12.92	2610.7980	5.24	109.3	0.00	0.01	0.01
1	9	”	”	12.92	2610.8720	5.96	124.2	0.00	0.01	0.01
2	1	228.6469	-17.2359	11.39	3190.0872	1.19	19.5	1.73	–	4.03
2	2	”	”	11.39	3190.1612	1.88	30.8	0.23	0.32	0.32
3	1	263.6591	-22.6800	12.34	3382.5890	1.19	24.1	1.06	–	3.82
3	2	”	”	12.34	3382.6630	1.28	26.1	1.20	3.57	3.57

TABLE 6: The most favourable events to detect the relativistic light deflection by the quadrupole gravitational field of Jupiter. This list is established for the MSL initialized as in Section 6.6. The dates are in days since J2010 TCB and the events happen respectively in February 2017, September 2018 and April 2019. All three noise models are considered in the last three columns: N_1, N_2 and N_3, with and without straylight (see Section 3.1). For the model N_2 and stars 2 and 3, the first observation occur closer to Jupiter limb than $5''$ and are eliminated. The event with star 2 is no longer important for this noise model. See also Appendix A.

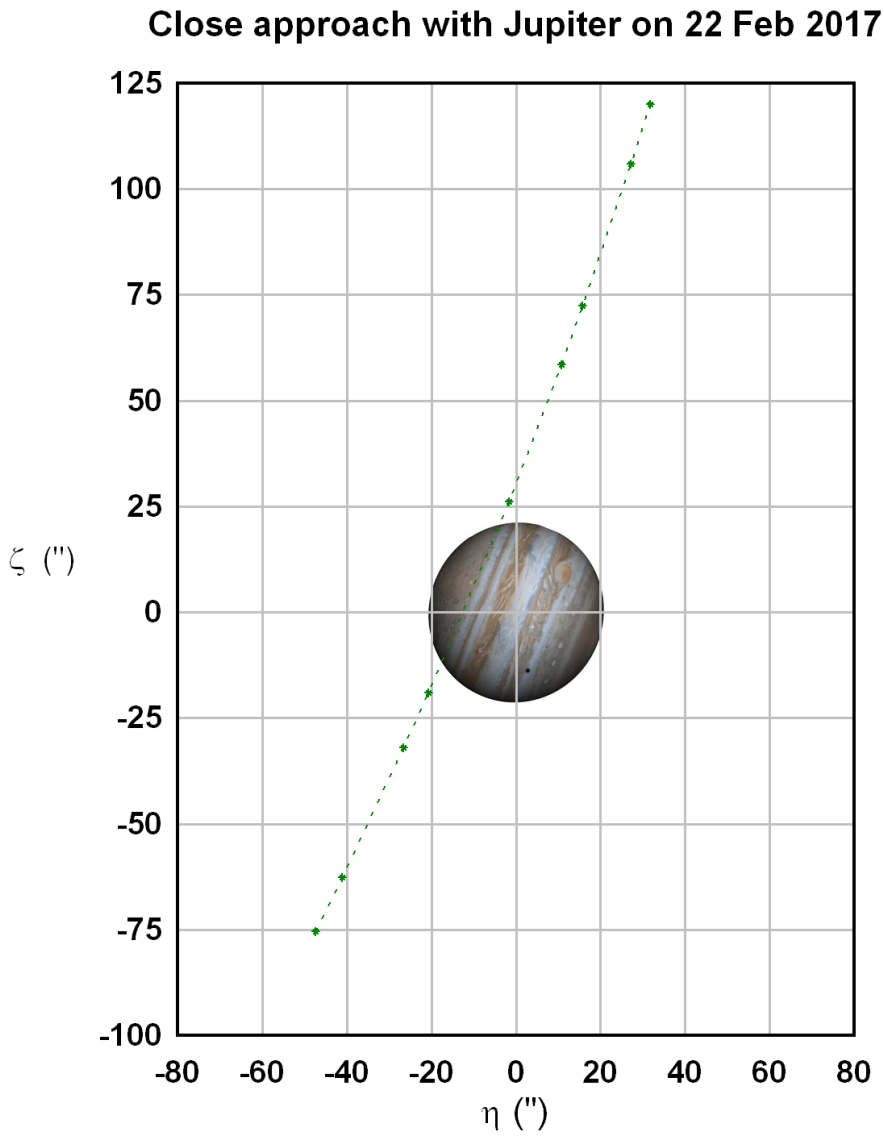


FIGURE 24: The close approach of February 2017 with a star of magnitude ≈ 13. With the recommended scanning law parameters, the star is observed 9 times in successive transits with Jupiter in the field. The light deflection is only significant for the 3 or 4 observations closest to Jupiter. This is a perfect opportunity for the differential method. η and ζ are the field coordinates (AL , AC) with origin at Jupiter. Jupiter is oriented in this frame to show the axis of symmetry of the deflection field. The relative motion of the star goes from bottom-left to top-right.

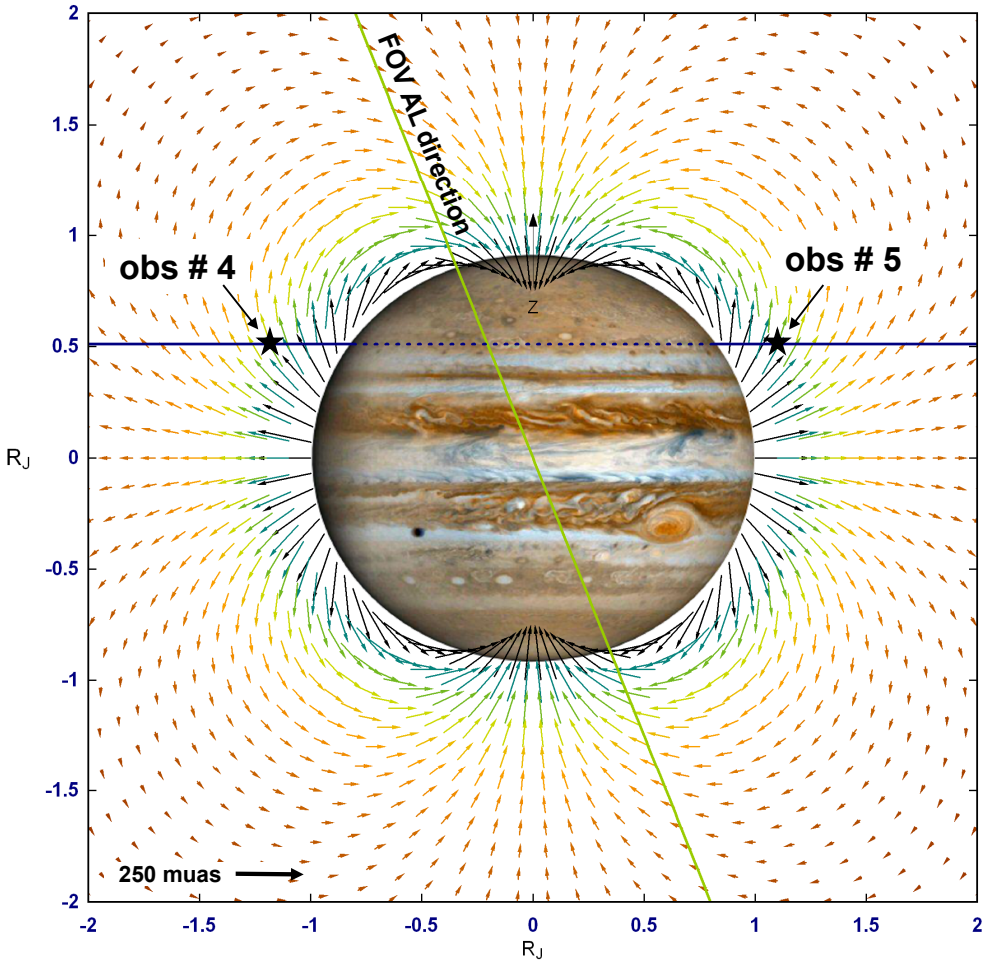


FIGURE 25: Close-up view to the event of February 2017 with the passage in front of a star of magnitude ≈ 13. The plot shows the two observations closest to Jupiter superimposed to the quadrupole deflection field. The useful signal is the projection of the deflection vector onto the AL direction. This explains why the 4th observations has a slightly better signature than the 5th, despite being farther from Jupiter.

8 Evaluation of possible spin phase maneuvers for the selected point

The spin phase maneuvers represent an active change of the spin phase of Gaia. By adjusting the Gaia spin phase at some precomputed moments of time one can hope to gather better observations of the quadrupole deflection of light due to Jupiter and as a result to reach higher s/n ratio for the science parameter. It was agreed between the SOC, MOC, DPAC and the Project Scientist that a few such maneuvers (no more than 6 in 5 years) will be possible during the mission (coupled with the orbital maintenance maneuvers).

Given the short time available between the decision that the spin phase maneuvers are at all possible and the launch, it was not possible to develop a full-fledged algorithm of spin-phase optimization (a serious optimization using e.g. genetic algorithms would be needed here). Two prototype algorithms are currently available (both implemented in *Mathematica*):

A. A quick empirical optimization algorithm for any given number of allowed spin phase maneuvers.

   The algorithm uses the idea of [GAREQ-relevant] an "event" (a passage of a star close to Jupiter), a "compound observation" (a sequence of Gaia observations of one and the same star within at most 30 hours), and an "observation" (a single Gaia observation of a star). Compound observations are considered as a single entity and cannot be broken into parts in this algorithm. The spin phase can be changed after any compound observation. Each compound observation is characterized by the total s/n ratio of all single observations composing that compound observation. First the sequence of compound observations is empirically found for which the total s/n ratio is maximal (this algorithm is not strict and can end up with a sub-optimal sequence of compound observations). The compound observations which involve spin phase maneuvers are then iteratively excluded (the compound observation with the least s/n ratio is excluded first) until the requested number of spin phase maneuvers is reached. Although the algorithm is not strict, numerical experiments showed its reasonably good performance.

B. An exact optimization algorithm for only one spin phase maneuver.

   This algorithm performs an explicit comparison of all possible spin phase maneuvers provided that only one spin phase maneuver is allowed during the mission. The algorithm is slow and feasible only if only one spin phase maneuver is allowed.

In both algorithms a time span of 10 hours is allocated for any spin phase maneuver: during these 10 hours all observations are considered as lost.

These algorithms were applied for the selected point to estimate what possibilities the spin phase maneuvers could give in the situation. The results are shown in Table 7 and on Figure 26. Table 8 shows the same data as Table 7, but represents the s/n ratios in terms of the increase

number of spin phase maneuvers	algorithm	noise model N_1	N_2	N_3
0	–	2.91430	6.69500	9.13470
1	A	2.91752	7.33243	9.88945
1	B	2.91752	7.50070	9.93752
6	A	2.96269	8.34076	10.75090
unlimited	A	3.00490 (20 maneuvers)	8.76399 (21 maneuvers)	11.25670 (22 maneuvers)

TABLE 7: The s/n ratios for the selected initial precession phase 52.66° for different number spin phase maneuvers. The algorithms A and B are described in Section 8, "–" means that a single optimal value for the initial spin phase was selected to give the maximal s/n ratio. The noise models N_1, N_2 and N_3 are described in Section 3.1.

number of spin phase maneuvers	algorithm	noise model N_1	N_2	N_3
0	–	2.91430	6.69500	9.13470
1	A	0.1%	9.5%	8.3%
1	B	0.1%	12.0%	8.8%
6	A	1.7%	24.6%	17.7%
unlimited	A	3.1% (20 maneuvers)	30.9% (21 maneuvers)	23.2% (22 maneuvers)

TABLE 8: The same data as in Table 7, but represented in terms of the s/n gains relative to the basis case with no spin maneuvers.

(gains) of the s/n ratio relative to the case without spin maneuvers. We see that for the straylight model (N_1) the total possible increase of the s/n ratio does not exceed 3.1%. For the other two noise models the gain is at most 31%. Given the uncertainty in the real noise model one cannot decide now if spin phase maneuvers make sense, but a positive message is that the GAREQ outcome does not depend too much on the implementation of the spin phase maneuvers.

On the other hand, it is possible that the final value of the scan rate (and the possibility that the scan rate is changed during the mission in order to further optimize Gaia performance) will lead to the necessity to use the spin phase maneuvers to catch the important GAREQ-relevant observations. The details will be given elsewhere as soon as the final scan rate is known (see also Section 9.3).

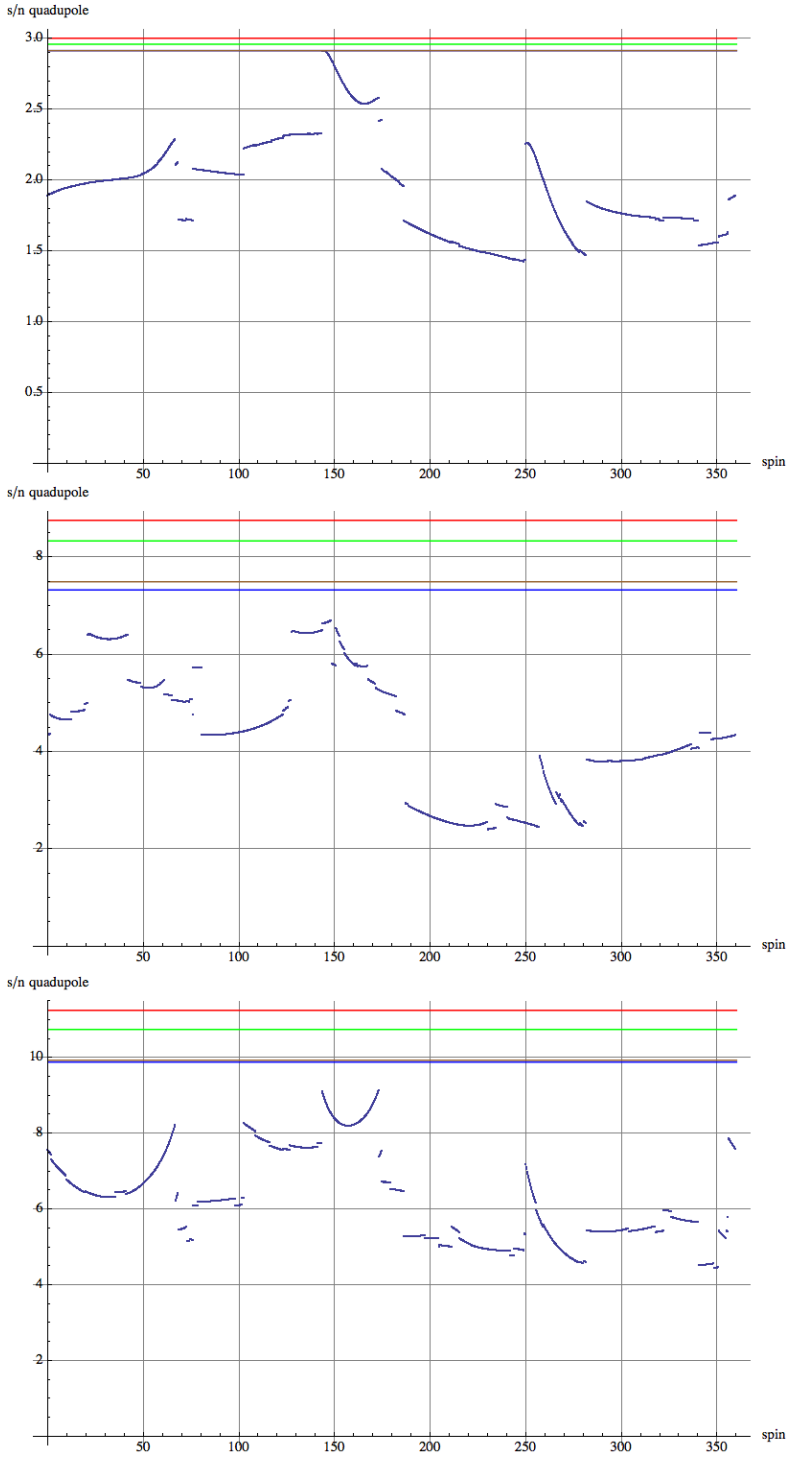


FIGURE 26: The s/n ratio for the selected initial precession phase 52.66° for different initial spin phases (horizontal axis) and three noise models: N_1 (upper pane), N_2 (middle pane) and N_3 (lower pane). The dark blue dots are the s/n ratio of the individual points of the 0.25° grid as function of the spin phase. The red line gives the s/n ratio for the full empirical optimization (unlimited number of maneuvers). The green line represents the s/n level of the empirical optimization for 6 maneuvers. The brown line is the exact optimization for 1 maneuver. The blue line is the empirical optimization with 1 maneuver (hidden behind the brown line for the straylight model).

9 Sensitivity to assumptions

9.1 Noise model

The above optimization is done with a certain number of assumptions and constraints. We don't know precisely how good bright stars could be observed very close to the surface of Jupiter. This won't be known before few actual observations are carried out during the first months of the mission. Jupiter is observable between 15 February and 25 May 2014 by Gaia and it may happens that it will be observed during commissioning. The question if Jupiter can be observed when Gaia is in EPSL can be answered as follows. Given the geometry of the EPSL and the motion of Jupiter, there are only two opportunities: on 15 February 2014 if the leading EPSL is used or on 25 May 2014 with the trailing EPSL. A simulation shows that there are actually 5 observations in the former instance and 7 on the latter. It will be interesting to have a look at the stars observed during at least one of these opportunities. This is purely indicative and a more detailed prediction will be made when the commissioning timeline is finalized with the corresponding scanning laws for each period. According to the current commissioning timeline on 25 May Gaia should already work in the "smooth" NSL (NSL smoothly attached to EPSL with no slew of Gaia in between). As for the 15 February it seems to be too early in the mission to allow any serious observations of Jupiter. It is still unclear if some observations of Jupiter could be done during the two NSL segments planned for the commissioning.

9.2 Gaia orbit

It is obvious that the close approaches between Jupiter and the stars should be computed in a Gaia-centric frame. Therefore, the geometry and timing of the events depend on the actual orbit of Gaia. The strength of a close approach measured by the efficiency at which one can detect the quadrupole light deflection is very sensitive to the closest distance measured in Jupiter radii. On the average the apparent radius of Jupiter is $20''$, meaning an error in the Gaia-centric direction of Jupiter of 1/10 of the radius amounts to $2''$, which is our closest accepted distance of observations to Jupiter limb. An error in the Gaia position of 7000 km, i.e one tenth of the Jupiter radius, would result into 2 arcsec in the predicted direction. This was the accuracy requirement agreed by MOC for the first predicted orbit of Gaia received on 30 December 2013 (MOC orbit file `ORB1_20131230_000001.txt`). This is a prediction with an agreed accuracy of 7000 km and we have no guarantee that Gaia would follow this orbit within this margin of 7000 km. If the deviation is (much) larger, obviously our optimal choice might be not so optimal, but this is the best one can do at the moment. However, if no unexpected event happens to Gaia one may reasonably think that this predicted orbit will be followed. We have a first hint that this will be the case with the delivery of the first operational orbit of Gaia delivered on 20 January 2014 (MOC orbit file `ORB1_20140120_000001.txt`), one month after launch and after both insertion maneuvers. The difference between the two orbits is shown in Fig. 27 and is never larger than 2500 km, well within our requirement.

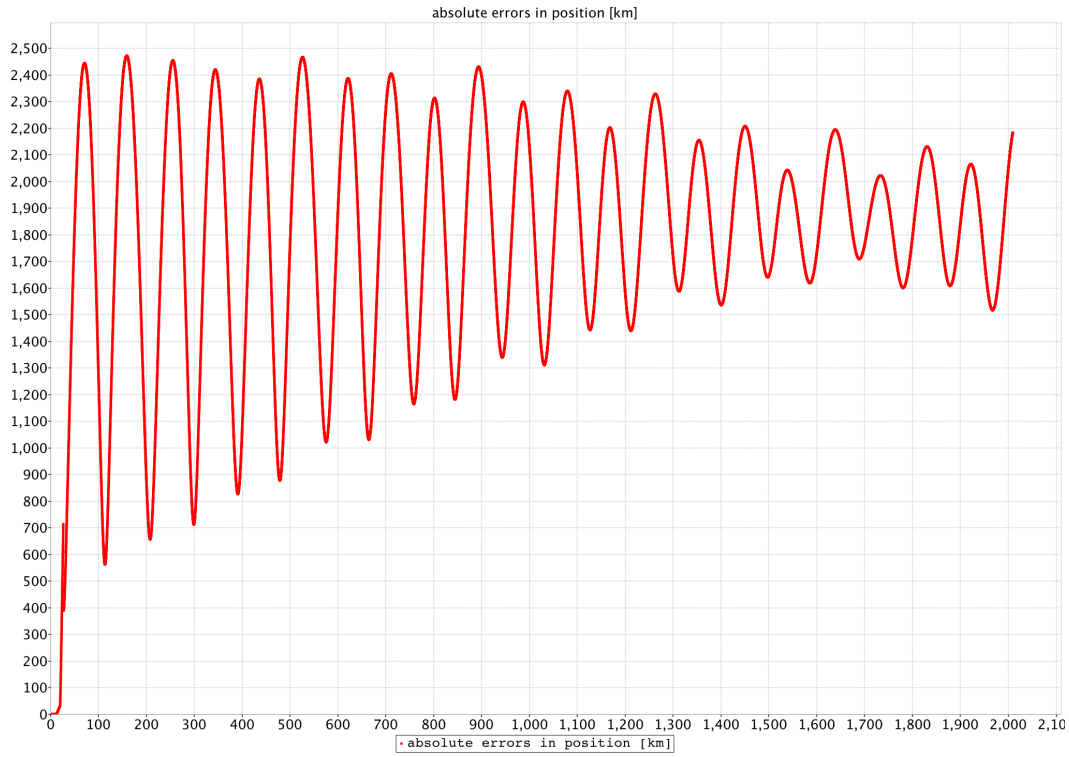


FIGURE 27: Difference in Gaia position between two releases of the Gaia orbit. The plot gives the distance between the two orbits delivered by MOC respectively on 30 December 2013 (MOC orbit file `ORB1_20131230_000001.txt`, the predicted orbit used in this work) and the Gaia orbit release after the insertion maneuvers (MOC orbit file `ORB1_20140120_000001.txt` released on 20 January 2014). The differences are never larger than 2500 km, well within SOGAR requirements.

9.3 Scan rate

Our optimization rests upon the computer representation of the scanning law and we have used a fixed scan rate, namely the reference value stored so far in the GPDB, with $\omega = 59.964185780301335$ arcsec/s in TCB. Still, a change of only 0.01 arcsec/sec leads to a shift of the spin phase of 86 degrees per year. A Jupiter crossing found in the nominal conditions, could be seen several hours before or after our computed value. As Jupiter moves typically at 5 mas/s, the distance to a star at a close approach may differ by several tens arcsec, sufficient to turn a favourable case into a much less interesting one, and vice versa. During this interval the scanning plane has also changed due to the precession motion and the Jupiter crossing does not happen in the same AC position. It may even be outside the FOV, and simply visible one revolution earlier or later, or a new one may become visible. Therefore it is important to look at how sensitive to the scan rate our selected precession is and ultimately whether the whole optimization works makes sense.

The optimization program was run in a special mode, where the precession phase is fixed to

$\nu_0 = 52.66°$ and a loop on the scan rate is added to explore now the configuration space in initial spin phase (as before) and in a limited range of scan rate. The exploration runs in two modes: a coarse mode from $\omega = 59.50$ to $\omega = 60.50$ arcsec/s with a step of 0.0002 arcsec/s and a fine mode from $\omega = 59.90$ to $\omega = 60.00$ arcsec/s with a step of 0.00005 arcsec/s. In both cases three noise models – N_1, N_2, N_3 – were used. The coarse mode corresponds to the range of scan rates used to search the optimal scan rate for Gaia. The fine mode allows us to reveal the intricate structure of the s/n ratio as function of the scan rate. The results for the fine mode are shown in Figs. 28–30 respectively for the noise models N_1, N_2 and N_3. The coarse mode shows similar behaviour for the whole range of the scan rate. Figure 31 shows, for the three noise models, the best s/n ratio for the fixed initial precession phase of $52.66°$ as function of the scan rate from $\omega = 59.50$ to $\omega = 60.50$ arcsec/s. For each value of the scan rate, the initial spin phase selected gives the maximal s/n ratio for the quadrupole deflection of light.

The good news is that for every value of the scan-rate in the explored range, there is always a choice of the spin phase producing a rather good detection sensitivity for our selected value of the precession initial phase. Looking in the vicinity of our optimal point, at $\omega = 59.964\ldots°$ and $\Omega_0 = 146°$, one first recovers our large s/n ratio and then one can follow the progressive shift of the optimal spin phase along the dark-red line. The slope of the shift in this diagram is rather well understood from the fact that the average time of observations of the three main events contributing to the signal is around 2018.4. At that time the shift would reach about $360°$ for an offset of the scan rate of about 0.0105 arcsec/s. This is more or less the slope of the strips seen in the plot. Said that, it is not possible to tell whether the good point in spin phase found for a scan rate different from our reference value is associated to the same three good stars. Checks done on few points seems to indicate a good stability in this feature (for example, for $\omega = 60.0$ arcsec/s it has been manually checked that the same three stars can be observed using $353.60°$) for the spin phase, but we are not in position to tell that this is true for every value of the scan rate. Moreover, a good point selected in this plot does not guarantee that it would correspond to the optimal value we would have selected had we explored the (initial precession phase, initial spin phase) configuration space with this scan rate.

In addition, Figure 31 demonstrates that depending on the scan rate the largest achievable s/n ratio by selecting the optimal initial spin phases varies by up to $\sim 30\%$. This means that for some values of the scan rate, some of the important observations cannot be observed together with some other important observations if only one initial spin phase is selected. It is clear that for a sequence of observations lasting at most several hours (see e.g. Table 6) only one can always – for any reasonable value of the scan rate – find the initial spin phase that guarantees that the sequence of observations is realized. However, if one considers two observations separated by years, one cannot be certain that for any value of the scan rate there exists an initial spin phase with which both observations are realized. We reach here the limitation of the optimization, or more precisely, this illustrates what is meant by a constrained optimization, specifically with loosely defined constraints.

The clean way out of this situation is to implement a few spin phase maneuvers during the

mission to match the spin phase, actual scan rate and the observations of interest. The spin phase maneuvers allow us to (slightly) improve the s/n ratio even for a fixed value of the scan rate (see Section 8). Given the fact that the scan rate can be even adjusted during the mission (to optimize Gaia performance further), it seems that spin phase maneuvers can become an important ingredient for the success of GAREQ. When the final in-flight value of the scan rate will become known, we will repeat the optimization process to assess the situation anew.

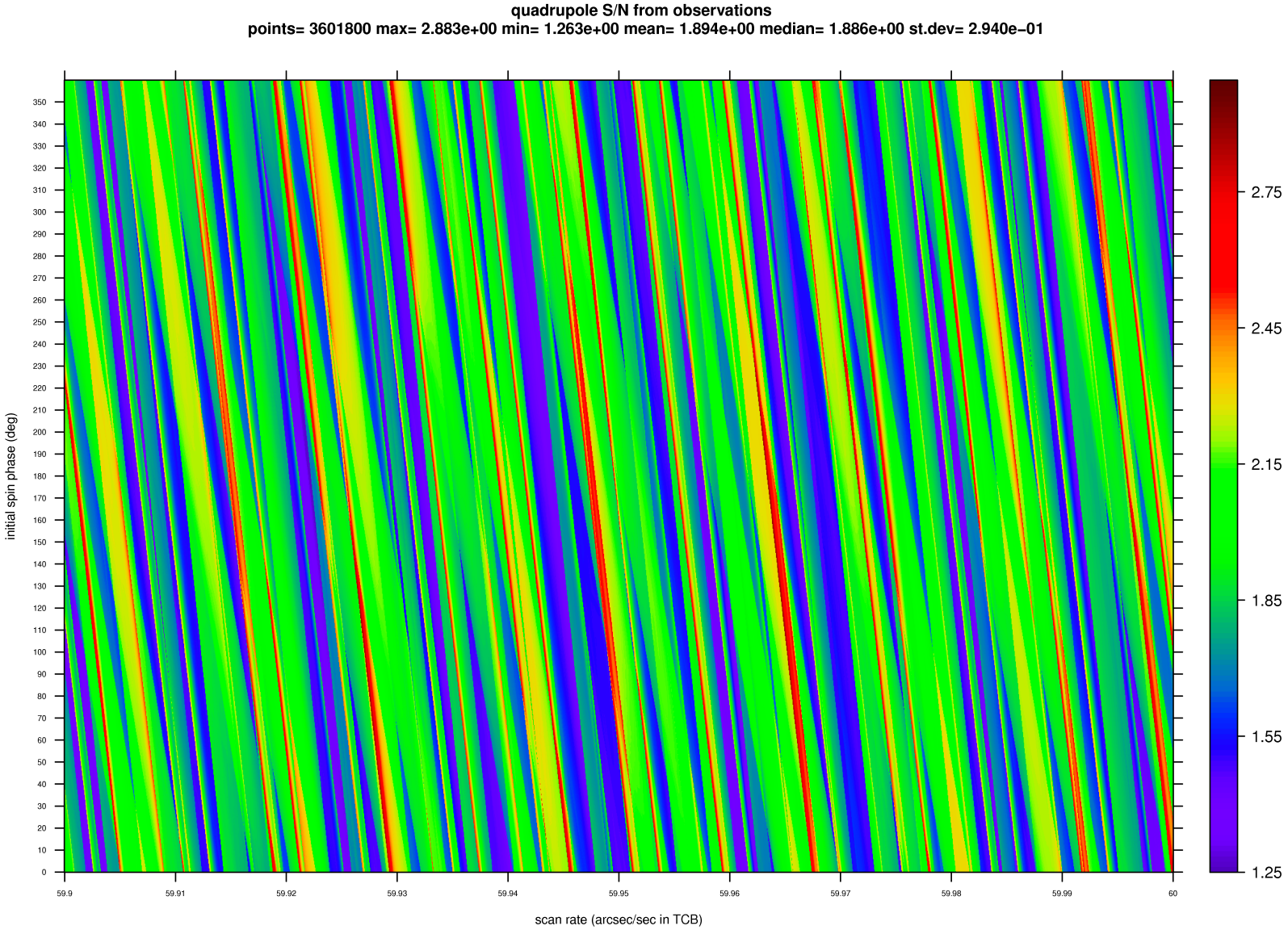


FIGURE 28: The colour-coded map of the s/n ratio for the fixed initial precession phase $\nu_0 = 52.66^\circ$ as function of scan rate and spin phases corresponding to the noise model N_1 and the full AC extension of the FOVs.

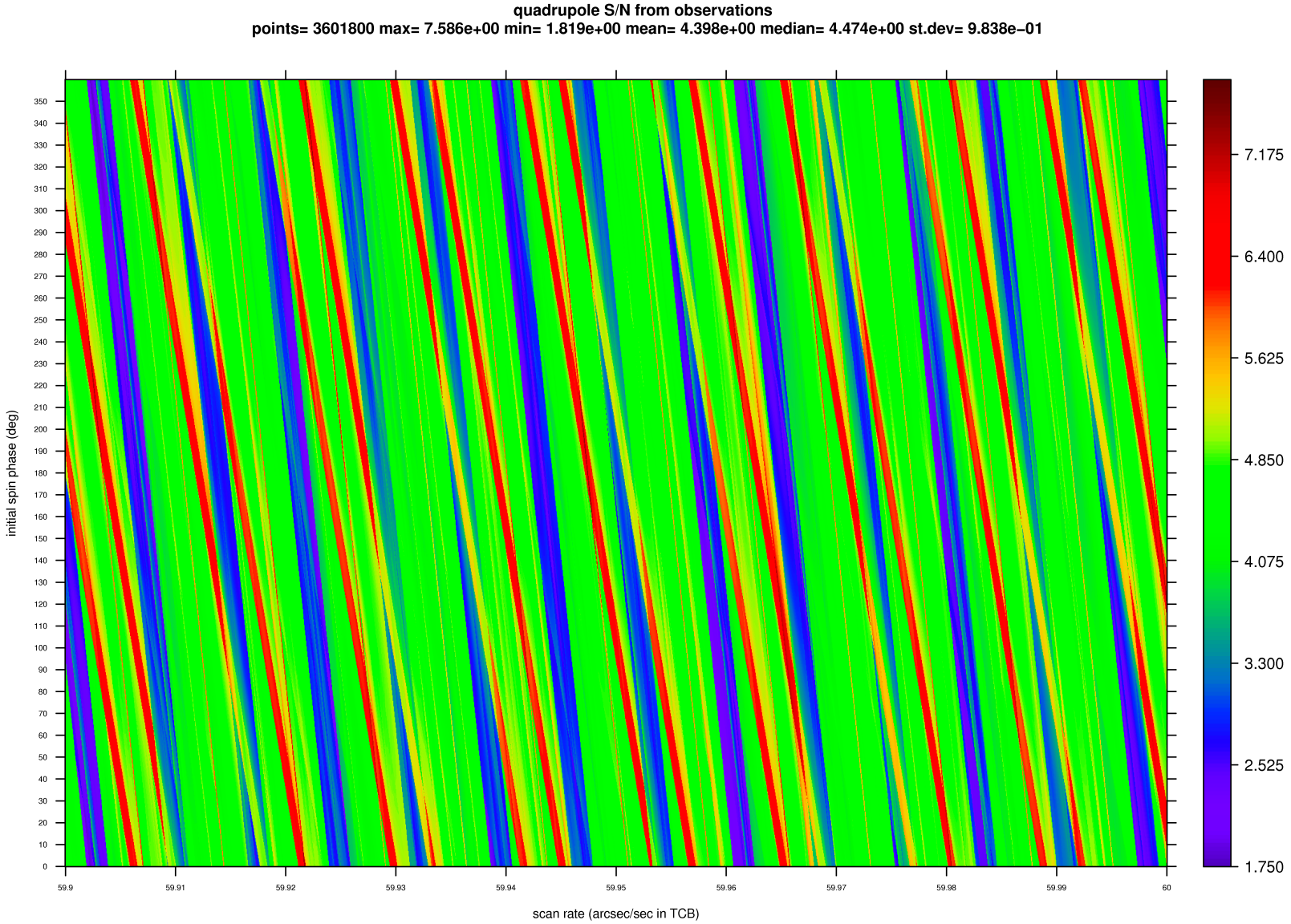


FIGURE 29: The colour-coded map of the s/n ratio for the fixed initial precession phase $\nu_0 = 52.66^\circ$ as function of scan rate and spin phases corresponding to the noise model N_2 and the full AC extension of the FOVs.

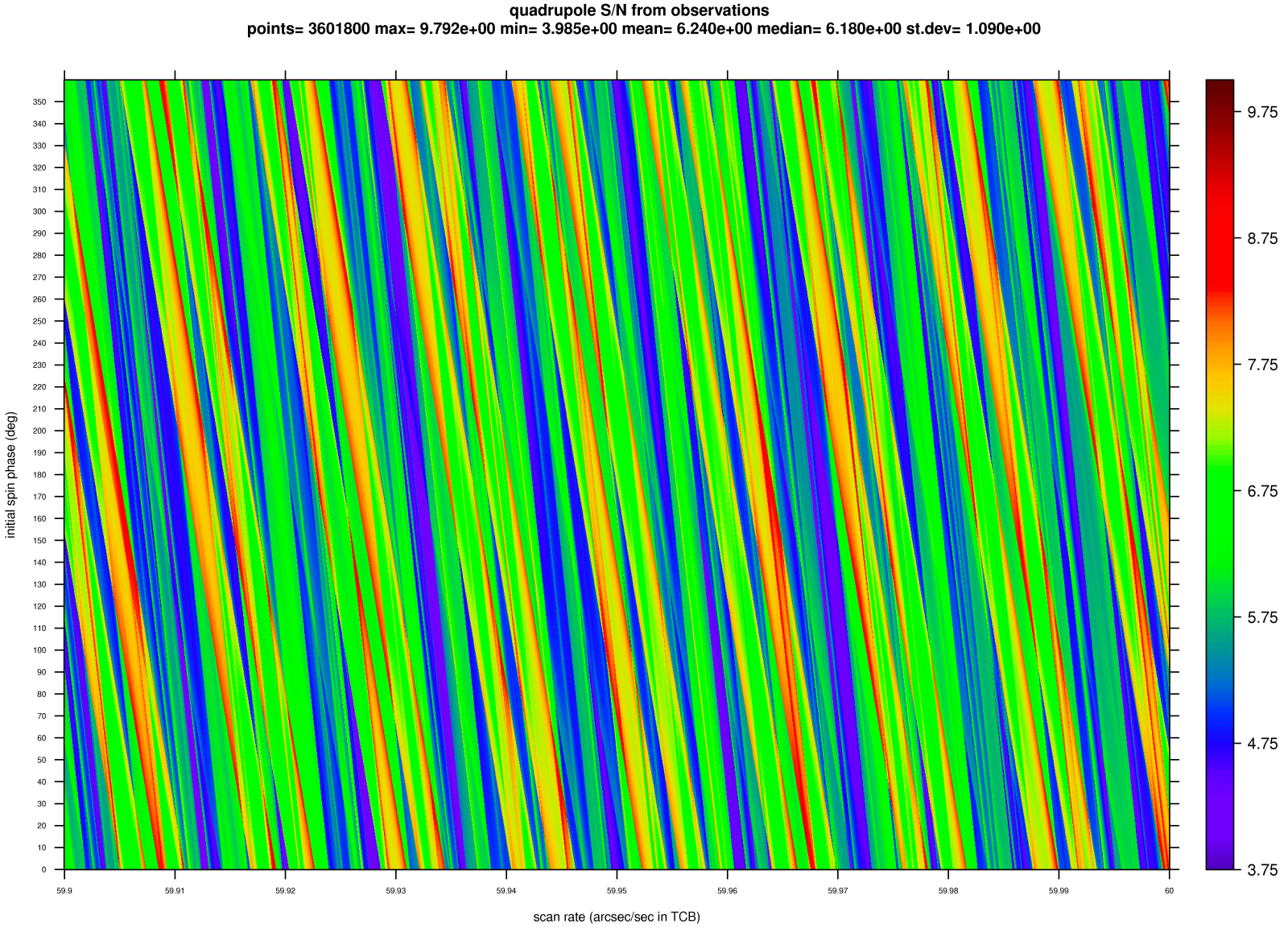


FIGURE 30: The colour-coded map of the s/n ratio for the fixed initial precession phase $\nu_0 = 52.66^\circ$ as function of scan rate and spin phases corresponding to the noise model N_3 and the full AC extension of the FOVs.

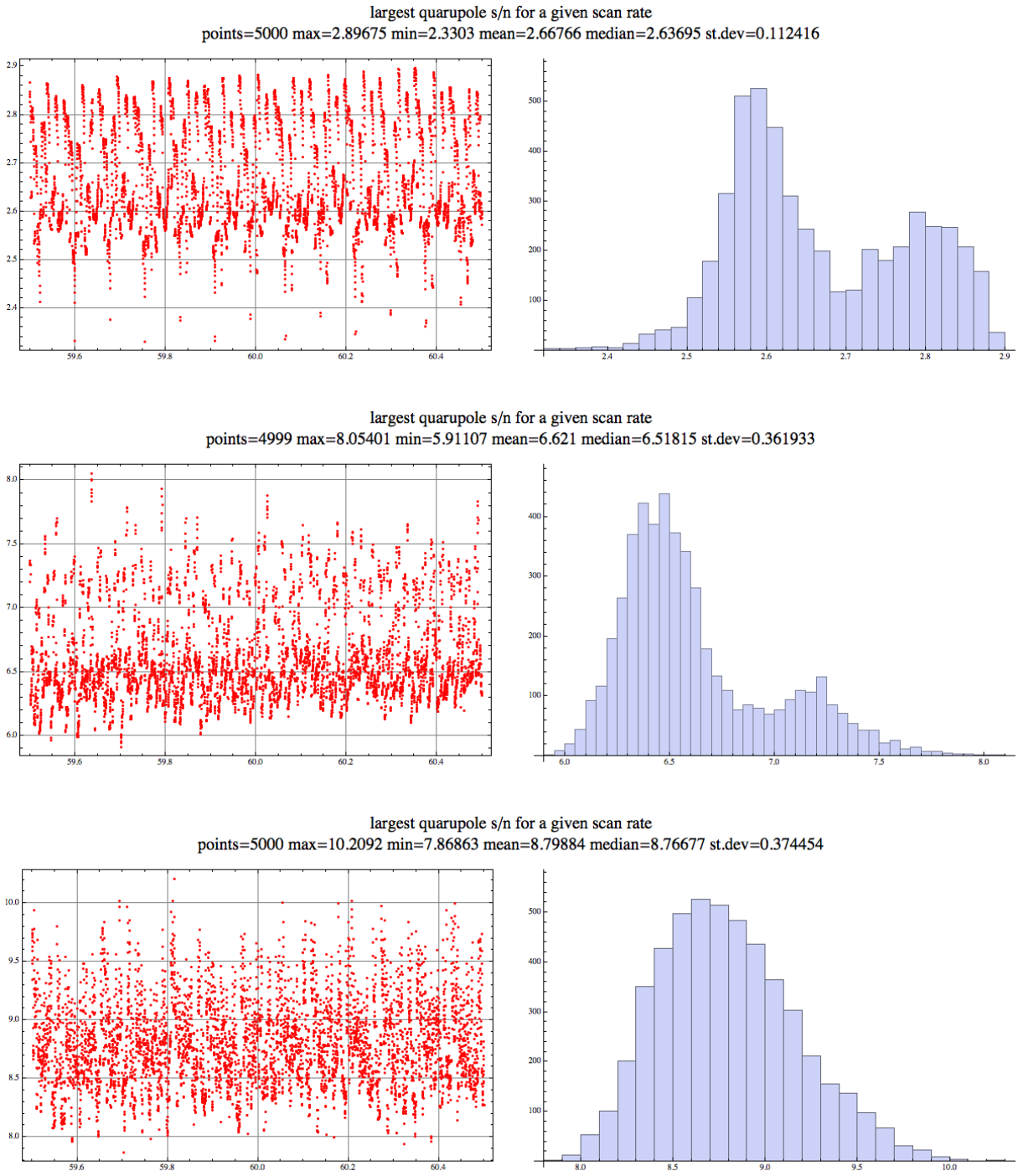


FIGURE 31: Best s/n ratio for the fixed initial precession phase of 52.66° as function of the scan rate from $\omega = 59.50$ to $\omega = 60.50$ arcsec/s. For each value of the scan rate, the initial spin phase was selected that gives the maximal s/n ratio for the quadrupole deflection of light. The ratios are shown for the three noise models: the upper plot is for N_1, the middle one for N_2 and the lower one for N_3.

10 Computational aspects and online repository

The two SOGAR codes, in Fortran and Java, produce voluminous output besides the merit function used to generate the maps. For each of our grid point in precession and spin phases, information is kept of each valuable close approach between Jupiter and one or more stars. Typically with a threshold in s/n of 0.1, there are between 20 to 40 close approaches per grid point, or $\sim 50000 - 100000$ per value of precession phase in our 0.2° resolution. For each star selected the timing, position of Jupiter and the star in the FOV, the monopole and quadrupole deflections and a couple of ancillary data are output. This cannot be handled on a case by case basis and several tools have been developed to access and exploit these massive results. This includes making the SOGAR output more compact using a python script (to speed up further processing), automatic statistical analysis and visualization using a dedicated R code, *Mathematica* code for the spin phase maneuvers, and shell scripts allowing to automatically parallelize the SOGAR computations on a specified grid in initial precession and spin phases and/or in scan rates. Specific scripts were also written to extract and analyze data just for a grid point.

We note that the SOGAR optimization performed in January 2014 required a total of 200 days of CPU time on latest-generation XEON processors. The computations were performed using 16–24 CPUs in parallel. The total amount of generated, automatically analyzed and visualized data is approximately 270GB in highly compressed form.

The repository of all relevant SOGAR runs can be accessed at:

`http://astro.geo.tu-dresden.de/archiveSogarRuns/Launch/`

The details of the structure and the content of the repository can be requested from the authors.

Acknowledgments

This report describes the results of the work which was prepared, discussed, organized and made possible by a large number of people from ESA, MOC, SOC and DPAC. Without contribution of all these people the SL optimization for GAREQ would have been impossible.

The Java version of SOGAR written by Christophe Ordénovic from OCA is gratefully acknowledged. Guillem Anglada-Escudé investigated, back in 2006–2007, the possibility to optimize the free NSL parameters for GAREQ and presented the results in a number of RRFWG and REMAT meetings and in his PhD thesis. His finding were largely confirmed by further investigations. Jos de Bruijne analyzed as early as 2008 possible competing requirements for the initial precession and spin phases. His conclusion that the GAREQ-related optimization is well possible from the operational point of view gave a crucial positive impulse to the development

of SOGAR. Jos de Bruijne also clarified a number of constraints of real operational schedule of Gaia and negotiated with the SOC and MOC to clarify the possibilities that could be used by GAREQ including the spin phase maneuvers. Hassan Siddiqui patiently explained to the SOGAR team the content and implications of the operational RSLS (Reference Scanning Law Schedule) generations. He also cleared up numerous questions with the MOC. Lennart Lindegren has drastically improved the performance of the MSL code in GaiaTools when using it on a grid of initial precession and spin phases. This has made possible the use of SOGAR with exactly the same scanning law implementation that will be used in operations. We also thank the MOC team for making substantial efforts to evaluate the feasibility of various GAREQ requirements and for the early delivery of the predicted Gaia orbit. Finally, members of the GAREQ team Ummi Abbas, Mariateresa Crosta and Mario Lattanzi participated in numerous discussions of the GAREQ and the SL optimization during the REMAT meetings.

SK was partially supported by the BMWi grants 50QG0901 and 50QG1402 awarded by the Deutsche Zentrum für Luft- und Raumfahrt e.V. (DLR).

A Summary of individual observations

Below you can find the list of individual observation grouped in the observing time and stars. Each line corresponds to one star with the right ascension, declination and magnitude given in the first three columns. The 4th column 'nObs' gives the number of observations of that star (irrespective of the s/n ratio of these individual observations). The 5th and 6th columns indicate the times (in years in TCB from 2010.0) of the first and last observation of the corresponding star. Finally the last three columns 'sn/N_i' gives the s/n ratio for the quadrupole deflection of light of all observations of the corresponding star taken together for the noise model N_i. All stars observed within 6 Jupiter angular radii from Jupiter and with magnitude 16 and brighter were taken into account. The stars discussed in Table 6 are indicated with '*'.

The stars and observations before 2017.0 give very small s/n ratios. They are indicated because these observations can be used to improve the noise model as well as to understand the details of the differential solution and to train the corresponding software.

Starting from 2017.0 all stars are shown that give the s/n ratio of 0.1 or greater for the noise model N_3. If the s/n ratio for models N_2 and N_3 are different, it means that some of the observations happen at an angular distance between $2''$ and $5''$ from the limb of Jupiter.

Further details are available upon request. Obviously, the details of observations will be updated as soon as more information on the real Gaia observational noise as well as the G magnitude of individual stars are available.

alpha	delta	mag	nObs	tBeg	tEnd	sn/N_1	sn/N_2	sn/N_3	
142.0357	15.5467	13.44	2	4.812639	4.812841	0.0368	0.0516	0.0516	
142.0456	15.5381	14.58	2	4.812639	4.812841	0.0552	0.0959	0.0959	
142.0753	15.5726	15.44	2	4.812639	4.812841	0.0117	0.0199	0.0199	
142.0753	15.5351	15.44	2	4.812639	4.812841	0.0148	0.0294	0.0294	
145.0572	14.7764	13.37	2	4.951536	4.951738	0.0352	0.0465	0.0465	
135.4606	17.8997	11.56	2	5.314388	5.314591	0.0099	0.0112	0.0112	
135.4681	17.8629	15.59	2	5.314388	5.314591	0.0401	0.1162	0.1162	
135.4736	17.8877	14.11	2	5.314388	5.314591	0.2523	0.4939	0.4939	
135.4912	17.8911	12.04	2	5.314388	5.314591	0.0618	0.0884	0.0884	
164.7689	7.9388	13.00	2	6.358919	6.359122	0.0450	0.0610	0.0610	
164.7877	7.9875	15.99	2	6.358919	6.359122	0.0120	0.0272	0.0272	
164.7899	7.9681	14.63	2	6.358919	6.359122	0.0915	0.2098	0.2098	
195.0826	-5.1361	12.82	1	6.903080	6.903080	0.0232	0.0335	0.0335	
195.0878	-5.1766	11.02	2	6.903080	6.903283	0.1354	0.1478	0.1478	
197.1528	-5.9735	15.97	3	6.939571	6.940256	0.0236	0.0715	0.0715	
197.1628	-5.9867	13.47	2	6.940053	6.940256	0.1780	0.3003	0.3003	
197.1658	-5.9576	15.29	3	6.939571	6.940256	0.0219	0.0434	0.0434	
201.4053	-7.3830	12.92	9	7.145236	7.148178	1.4233	4.6049	4.6049	*
201.3802	-7.3713	15.76	8	7.146606	7.149345	0.1562	1.1828	1.1828	
201.3462	-7.3442	14.52	8	7.148660	7.150917	0.1130	0.2038	0.2038	
201.3044	-7.3464	15.84	9	7.150030	7.152972	0.0760	0.2201	0.4339	
192.5934	-3.7942	13.86	2	7.406192	7.406395	0.1160	0.1728	0.1728	
194.5556	-4.8630	13.83	2	7.550567	7.550769	0.1075	0.1677	0.1677	
230.8734	-17.3750	13.45	2	8.161730	8.161932	0.1334	0.4995	0.4995	
230.8851	-17.3815	15.77	2	8.161730	8.161932	0.0562	0.5353	0.5353	
221.5398	-14.8296	15.60	6	8.465117	8.467374	0.1266	0.5326	0.5326	
221.5150	-14.7999	15.64	5	8.465802	8.467374	0.0679	0.1923	0.1923	
221.5050	-14.8061	15.19	3	8.466487	8.467374	0.1735	1.3137	1.3137	
221.2474	-14.7585	15.92	4	8.481071	8.482238	0.0782	0.6526	0.6526	
221.2496	-14.7505	13.57	4	8.481071	8.482238	0.5504	1.6252	1.6252	
228.6469	-17.2359	11.39	2	8.733983	8.734185	1.7459	0.3208	4.0463	*
258.8124	-22.4220	15.43	2	9.119388	9.119591	0.1394	1.1328	1.1328	
258.8311	-22.4076	14.82	2	9.119388	9.119591	0.1131	0.3113	0.3113	
258.8355	-22.4212	14.30	2	9.119388	9.119591	0.1039	0.2573	0.2573	
262.1152	-22.6172	15.24	1	9.187815	9.187815	0.0749	0.2091	0.2091	
262.1347	-22.6209	15.23	1	9.187815	9.187815	0.1120	0.0000	1.0330	
263.6451	-22.6875	15.26	2	9.261024	9.261227	0.0588	0.1269	0.1269	
263.6591	-22.6800	12.34	2	9.261024	9.261227	1.5947	3.5679	5.2316	*
263.6609	-22.6990	14.03	2	9.261024	9.261227	0.2683	0.4764	0.4764	
263.6629	-22.7001	15.60	2	9.261024	9.261227	0.0544	0.1528	0.1528	
263.6648	-22.6736	15.71	2	9.261024	9.261227	0.0779	0.2744	0.2744	
263.6671	-22.6780	15.88	2	9.261024	9.261227	0.1187	0.8092	0.8092	
263.6760	-22.6922	15.12	2	9.261024	9.261227	0.0854	0.2197	0.2197	
263.6806	-22.6852	14.34	2	9.261024	9.261227	0.1226	0.2143	0.2143	